The Meteoritical Society

Meteoritics & Planetary Science 46, Nr 2, 177–198 (2011)
doi: 10.1111/j.1945-5100.2010.01142.x

Cosmogenic radionuclides in L5 and LL5 chondrites from Queen Alexandra Range, Antarctica: Identification of a large L/LL5 chondrite shower with a preatmospheric mass of approximately 50,000 kg

K. C. WELTEN[1*], M. W. CAFFEE[2,3], D. J. HILLEGONDS[2], T. J. McCOY[4], J. MASARIK[5], and K. NISHIIZUMI[1]

[1]Space Sciences Laboratory, University of California, Berkeley, California 94720–7450, USA
[2]Center for Accelerator Mass Spectrometry, Lawrence Livermore National Laboratory, Livermore, California 94550, USA
[3]Department of Physics, Purdue University, West Lafayette, Indiana 47907, USA
[4]Department of Mineral Sciences, U.S. Museum of Natural History, Smithsonian Institution, Washington, District of Columbia 20560–0119, USA
[5]Department of Nuclear Physics, Comenius University, Mlynska dolina F/1, Sk-84248 Bratislava, Slovakia
[*]Corresponding author. E-mail: kcwelten@berkeley.edu

(Received 14 January 2010; revision accepted 15 October 2010)

Abstract–The collection of approximately 3300 meteorites from the Queen Alexandra Range (QUE) area, Antarctica, is dominated by more than 2000 chondrites classified as either L5 or LL5. Based on concentrations of the cosmogenic radionuclides ^{10}Be, ^{26}Al, ^{36}Cl, and ^{41}Ca in the metal and stone fraction of 16 QUE L5 or LL5 chondrites, we conclude that 13 meteorites belong to a single meteorite shower, QUE 90201, with a large preatmospheric size and a terrestrial age of 125 kyr. Members of this shower have properties typical of L (e.g., pyroxene composition) and LL chondrites (e.g., metal abundance and composition), as well as properties intermediate between the L and LL groups (e.g., olivine composition), and is thus best described as an L/LL5 chondrite. Based on comparison with model calculations, the measured radionuclide concentrations in the metal and stone fractions of QUE 90201 indicate irradiation in an object with a preatmospheric radius of approximately 150 cm, representing one of the largest chondrites known so far. Based on the abundance of small L5 and LL5 chondrites at QUE and their distinct mass distribution, we conclude that the QUE 90201 shower includes up to 2000 fragments with a total recovered mass of 60–70 kg, <1% of the preatmospheric mass of approximately 50,000 kg. The mass distribution of the QUE 90201 shower suggests that the meteoroid experienced catastrophic atmospheric fragmentation(s), either because it was a fragile object or it had a high entry velocity.

INTRODUCTION

In the past three decades, more than 30,000 meteorites have been recovered from the Antarctic continent. Most of these meteorites were found in high concentrations on relatively small areas of exposed glacier ice (blue ice) and in nearby moraines. One of the major meteorite concentrations in Antarctica is an area known as Queen Alexandra Range (QUE). After the first finds during reconnaissance trips in 1986 and 1987, the blue ice surfaces at QUE were extensively examined by the U.S. Antarctic Search for Meteorites in 1990, 1993, 1994, 1997, 1999, and 2002, with a total yield of 3358 specimens (Cassidy et al. 1992; Harvey 2003). From the 1990 and 1993 collections, a large number of L5 chondrites were classified by Brian Mason; based on petrologic studies alone more than 120 of these were tentatively paired as part of the QUE 90201 shower (Grossman 1994; Grossman and Score 1996). In 1997 and 1999, ANSMET field parties returned almost 2000 individual meteorites, with approximately 70% classified by one of us (T. J. M.) and colleagues at the Smithsonian

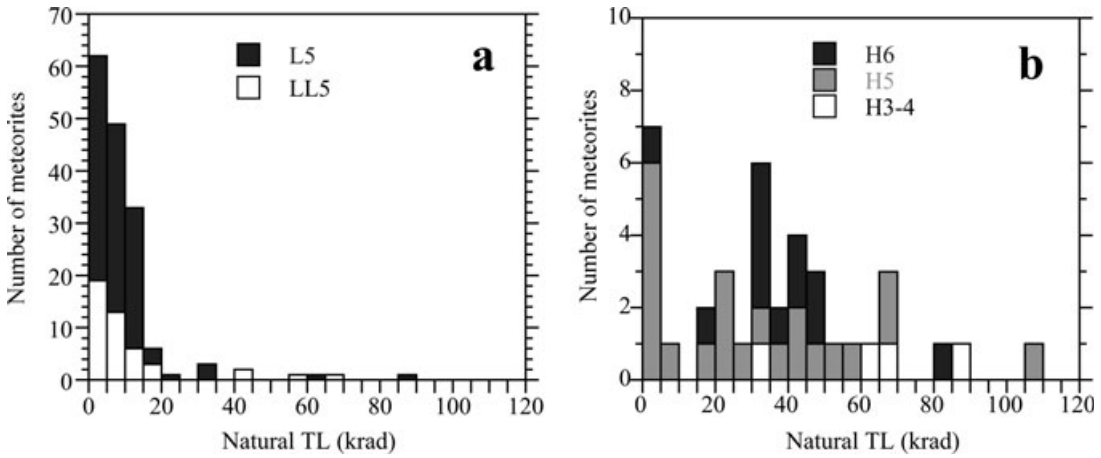

Fig. 1. Natural thermoluminescence levels in a) L5 + LL5 chondrites and b) H3-6 chondrites from Queen Alexandra Range (data from Benoit et al. [2000] and references therein). Note the different scale of the *Y*-axis in panels (a) and (b).

as LL5 chondrites. As only 1.5% of all documented meteorite falls are LL5 chondrites (Grady 2000), the high percentage of LL5 chondrites (~43%) in the QUE meteorite collection suggests that many of these LL5 chondrites belong to one (or a few) large pairing groups (e.g., McBride 2002).

The high degree of pairing among QUE L5 and LL5 chondrites is also supported by their low natural thermoluminescence (NTL) levels (<20 krad), which are typical for approximately 95% of the L5 and LL5 chondrites, whereas only one of four H chondrites from the QUE area have such low NTL levels (Fig. 1, based on data from Benoit et al. 2000). There is, however, considerable uncertainty about the number of pairing groups among the QUE L5 chondrites. While petrologic data suggested one pairing group of 120 members, Benoit et al. (2000) proposed at least three separate pairing groups based on the NTL data: 39 members with NTL levels of <5 krad, 55 members with NTL levels of 5–16 krad, and 3 members with NTL levels of 32–35 krad. However, they did not exclude the possibility that the first two pairing groups are related or that the second pairing group represents more than one separate fall (Benoit et al. 2000). In addition, many of the QUE LL5 chondrites show very similar NTL values as the L5 chondrites, which raises the question whether low NTL levels are a unique feature of QUE meteorites or indicate a large L5–LL5 chondrite shower.

A robust method for identifying paired meteorites relies on the concentrations of cosmogenic radionuclides, which provide information on the exposure history, preatmospheric size, and terrestrial age of a meteorite. This method proved very successful in identifying paired fragments of a large and heterogeneous Antarctic H3–6 chondrite shower, especially when other pairing criteria, such as petrologic type and cosmogenic and solar noble gas contents, were inconclusive (Welten et al. 2006; Leya et al. 2009). As part of a terrestrial age survey, we measured the ^{36}Cl concentrations in the metal fraction of approximately 80 ordinary chondrites from the QUE collection, as well as ^{10}Be in approximately 50 of these. About one-third of the chondrites shows ^{36}Cl concentrations <15 dpm kg^{-1} (metal), relative to typical concentrations of 20–25 dpm kg^{-1} for the metal fraction in chondrite falls. These low ^{36}Cl concentrations can either be due to high terrestrial ages or high shielding conditions. Most of the QUE meteorites with low ^{36}Cl concentrations also show low ^{10}Be concentrations in the metal phase, indicating significant shielding in a large preatmospheric object. Interestingly, meteorites with low ^{10}Be and ^{36}Cl concentrations mainly include L5 and LL5 chondrites. Preliminary radionuclide concentrations of five L5 and two LL5 chondrites from the QUE collection suggested that the L5 and LL5 chondrites are most likely part of a single L/LL5 chondrite shower with a large preatmospheric size (Welten et al. 2002). The main purpose of this article is to identify how many individual chondrite falls are represented by the QUE L5 and LL5 chondrites and to constrain the preatmospheric size of the largest shower(s).

Identifying the presence of large chondrite showers in Antarctic meteorite collections is not only important to constrain the number of independent meteorite falls at each meteorite stranding site, but is also relevant to determine the frequency and associated hazards of large stony meteorite impacts (Hills and Goda 1993; Bland and Artemieva 2006). Although objects larger than 1 m in radius enter Earth's atmosphere approximately 10 times per year (Bland and Artemieva 2006), we only

know of a few chondrites with a preatmospheric radius larger than 1 m in our meteorite collections, including Tsarev (Nagai et al. 1993), Gold Basin (Kring et al. 2001), and Northwest Africa (NWA) 869 (Metzler et al. 2008), which are all showers with many hundreds to thousands of fragments. While large meteorites (>1000 kg) are relatively common among irons, they are rare among stones. Because of the lower physical strength of stones, large stone meteoroids are more likely than irons to experience atmospheric fragmentation, and thus tend to produce large showers rather than large surviving stones (Bland and Artemieva 2006). It is thus plausible that some of the largest chondrites in our meteorite collections are "hidden" among large showers of relatively small fragments.

Secondly, cosmogenic nuclide studies of large chondrite showers are useful to test model calculations for cosmogenic nuclide production rates (Nagai et al. 1993; Leya et al. 2000; Masarik et al. 2001; Leya and Masarik 2009). These models generally provide good agreement with experimental data for small to medium-sized objects, with radii of 10–50 cm (e.g., Leya et al. 2001), but have not been tested thoroughly for chondritic objects larger than 1 m in radius. A detailed study of cosmogenic nuclides in the large Gold Basin L chondrite, with a preatmospheric radius of 3–5 m, suggested that at high shielding, some of the calculated production rates may differ by as much as 50% relative to the measured production rates (Welten et al. 2003). To further improve these model calculations for large objects, more cosmogenic nuclide studies of large chondrites are needed to test cosmogenic nuclide production rate models for objects with radii of 1–5 m.

Finally, large chondrite showers are also interesting for cosmic-ray exposure age (CRE) studies, as they tend to show complex exposure histories, i.e., they were exposed on the surface of large meteoroids ($R > 10$ m) or asteroids before being ejected into space as a meter-sized object. Well-documented examples of large chondrites with complex histories include Jilin (Honda et al. 1982), Bur Gheluai (Vogt et al. 1993), Jiddat al Harasis 073 (Huber et al. 2008), Tsarev (Nagai et al. 1993), and Gold Basin (Welten et al. 2003). These complex exposure histories are intriguing, because they are rare (<5%) among smaller chondrites. For meteorite falls and meteorite finds from hot deserts, these large showers are easy to identify based on the strewn field pattern. However, for Antarctic meteorites, which are usually not found in their original fall location, this identification requires several lines of evidence, including cosmogenic nuclide studies.

This paper consists of four parts: (1) study of the compositional variations among the QUE L5 and LL5 chondrites, based on bulk metal as well as olivine and pyroxene compositions; (2) determining the terrestrial age of selected QUE L5 and LL5 chondrites, based on the measured concentrations of the cosmogenic radionuclides ^{10}Be (half-life = 1.36×10^6 yr), ^{26}Al (7.05×10^5 yr), ^{36}Cl (3.01×10^5 yr), and ^{41}Ca (1.04×10^5 yr) in the metal phase; (3) comparison of measured radionuclide concentrations in the metal and stone fractions of QUE 90201 shower with calculated production rates to determine the preatmospheric size and irradiation depth of the samples. For calculating cosmogenic nuclide production rates, we used a purely physical model (Masarik and Reedy 1994a) that was previously used for the large Gold Basin meteorite (Welten et al. 2003) as well as a semiempirical model (Nagai et al. 1993) that was used for the large Brenham pallasite (Honda et al. 2002); and (4) evaluating the degree of pairing among QUE chondrites and obtain information on the atmospheric fragmentation process of the QUE 90201 meteoroid.

EXPERIMENTAL METHODS

Sample Selection and Preparation

We selected 23 ordinary chondrites from the QUE collection, with 13 classified as L5, eight as LL5, one as LL4, and one as LL6 (Table 1). Six of the selected meteorites are considered to be part of the QUE 90201 pairing group. The chondrites selected for this study are from a variety of blue ice surfaces and moraines within the QUE stranding area, which is described in more detail by Harvey (2003). The meteorites range in mass from 3 g to approximately 5 kg, and show a wide range in the degree of weathering, varying from A (minor rustiness) to C (severe rustiness). Natural TL levels were measured previously in 12 of the 23 selected samples and range from 0.6 to 161 krad (Benoit et al. 2000).

Samples weighing 1.5–3.2 g were gently crushed in an agate mortar and the metal was separated with a magnet. The metal was ultrasonically agitated for 15–30 min in 0.2 N HCl and concentrated HF to remove attached troilite and silicates, respectively. Purified metal samples of 35–100 mg were dissolved in 1.5 N HNO_3, along with a carrier solution containing approximately 2 mg of Be, Al, and Ca, and approximately 5 mg of Cl. After complete dissolution of the metal, aliquots were taken for chemical analysis by atomic absorption spectrometry (AAS). For the nonmagnetic fraction, we dissolved an aliquot of approximately 120 mg in concentrated HF/HNO_3 along with a carrier solution containing approximately 5 mg of Be and Cl. After complete dissolution of the silicates, aliquots were taken for chemical analysis by AAS.

Table 1. General description and metal composition of selected L5 and LL5 chondrites from the QUE collection.

QUE	Type	Mass	Location	WC	%Fa	NTL	Bulk metal	Mg	Fe	Ni	Co	Silicate
90201	L5	1282.5	FBI	A/B	26	8.0	3.7	0.019	76	24.0	1.02	0.11
90205	L5	458.5	FBI	A/B	26	0.6	3.9	0.013	71	26.7	1.16	0.08
90207	L5	366.9	FBI	A/B	26	9.7	3.5	0.013	75	25.8	1.17	0.08
90218	L5	926.5	FBI	A/B	26	34.0	4.9	0.059	75	23.5	1.11	0.35
90286	L5	429.3	FBI	B	–	5.9	4.0	0.044	73	25.3	1.13	0.26
93020	L5	597.3	CNI	A/B	27	11.6	4.2	0.021	76	22.8	1.07	0.12
93021	L5	2100.3	PI	B/C	23	161.0	8.7	0.057	88	11.4	0.65	0.34
93050	LL4	145.0	MM	B/C	28	–	2.5	0.115	76	21.8	1.02	0.68
94247	LL6	86.1	FRF	A/B	–	4.0	2.5	0.428	72	21.9	1.07	2.52
97013	LL5	706.0	PI	C	30	40.7	6.9	0.037	75	26.2	0.52	0.22
97017	LL5	305.9	MM	A	32	3.5	4.3	0.144	75	23.2	1.13	0.85
97028	LL5	910.9	MM	A	31	41.3	1.6	0.166	63	31.6	1.52	0.98
97429	LL5	39.9	MM	B/C	28	–	2.3	0.036	74	25.5	1.23	0.21
97463	LL5	3.0	MM	B/C	–	–	3.5	0.088	75	25.4	1.28	0.52
97998	LL5	3.0	GNI	B/C	28	–	3.2	0.024	75	24.7	1.34	0.14
971003	LL5	52.4	MM	B	–	–	3.1	0.072	74	26.2	1.34	0.42
93182	L5[a]	135.5	PI	B/C	–	–	15.5	0.052	86	11.7	0.46	0.30
97022	L5[a]	206.4	GN	B/C	22	35.8	12.5	0.025	89	9.0	0.50	0.15
97039	L5[a]	322.4	MM	B	23	–	13.8	0.037	87	10.3	0.47	0.21
97047	L5[a]	183.7	MM	C	22	–	10.8	0.055	87	10.1	0.45	0.33
99010	L5[a]	1293.4	TE	C	–	–	14.0	0.103	87	10.3	0.47	0.60
99013	L5[a]	814.2	TE	C	–	–	6.9	0.005	86	9.8	0.43	0.03
99017	LL5[a]	4999.0	GN	B	–	–	12.3	0.053	87	10.8	0.47	0.31

Note: Recovered mass (g), find location, olivine composition (in mole% fayalite), weathering category (A–B–C), and natural TL values (in krad) are from Meteoritical Bulletins, No. 76, 79, 82–85. Bulk metal contents and Mg, Fe, Ni, and Co concentrations in metal (in wt%) are from this work. The amount of silicate contamination in the metal (in wt%) is estimated from the measured Mg concentration by assuming the silicates contain 17 wt% Mg.

CNI = Central Nunataks Icefield; FBI = Foggy Bottom Icefield; FRF = Footrot Flats; GNI = Goodwin Nunataks Icefields; MM = Mare Meteoritics; PI = Pwellam Icefield; TE = Tail's End Icefield (Harvey 2003).

[a]Metal composition suggests that these meteorites are H chondrites (Welten and Nishiizumi 2007).

Chemical Analysis

We measured the concentrations of Mg, Fe, Co, and Ni in aliquots of the dissolved metal sample and of Mg, Al, K, Ca, Fe, and Ni in the dissolved silicate fraction. We used flame AAS using a Perkin Elmer AA 3300. The presence of Mg in the dissolved samples indicates contamination of the metal with silicates. The measured Mg concentration in most metal samples indicates silicate contaminations of <0.5 wt%, whereas two metal samples contain up to 1.0 wt% silicate (Table 1). Although the absolute concentrations of Ni and Co in the metal vary by a factor of 2–3, the Ni/Co ratio in 17 of the 18 metal samples is relatively constant at 21 ± 2 (Table 2). This ratio is very close to the chondritic ratio of 20 (Wasson and Kallemeyn 1988) indicating that leaching with HF did not alter the metal composition significantly, as was also found in previous studies (Kong and Ebihara 1997). On the other hand, the Ni/Co ratio of approximately 50 in the metal fraction of QUE 97013 indicates that the prolonged HF leaching (~45 min) of this metal sample led to preferential dissolution of kamacite (low-Ni, high-Co metal) over taenite (high Ni, low-Co metal), thus increasing the Ni and depleting the Co concentration in the remaining metal.

Radionuclide Measurements

Subsequent sample preparation steps to separate Be, Al, Cl, and Ca were performed following the procedures described by Welten et al. (1999, 2001a). Concentrations of ^{10}Be, ^{26}Al, ^{36}Cl, and ^{41}Ca were measured by accelerator mass spectrometry (AMS). The majority of the QUE samples was measured at Lawrence Livermore National Laboratory (Davis et al. 1990), while measurements of ^{10}Be, ^{26}Al, and ^{36}Cl in QUE 93050, 97028, and 94247 were performed at Purdue's PRIME Laboratory (Sharma et al. 2000). Measured ^{10}Be/Be, ^{26}Al/Al, ^{36}Cl/Cl, and ^{41}Ca/Ca ratios are corrected for isobaric interferences and chemical blanks and normalized to ^{10}Be, ^{26}Al, ^{36}Cl, and ^{41}Ca AMS standards (Sharma et al. 1990; Nishiizumi et al. 2000, 2007; Nishiizumi 2004). Although ^{10}Be, ^{26}Al, and ^{36}Cl concentrations were measured at two different AMS laboratories, we used the same AMS standards to

Table 2. Radionuclide concentrations (in dpm kg^{-1}) in the metal phase of QUE L5 and LL5 chondrites.

QUE	Type	^{10}Be	^{26}Al	^{36}Cl	^{41}Ca	^{36}Cl/^{10}Be[a]	^{41}Ca/^{36}Cl	T36	T41	T(avg.)
Members of QUE 90201 L/LL5 chondrite shower										
97998	LL5	3.64 ± 0.11	2.48 ± 0.07	14.0 ± 0.3	10.2 ± 1.0	4.00 ± 0.15	0.73 ± 0.07	100 ± 26	97 ± 26	99 ± 18
97463	LL5	3.57 ± 0.07	2.44 ± 0.10	13.1 ± 0.3	8.1 ± 0.5	3.82 ± 0.10	0.62 ± 0.04	126 ± 21	137 ± 20	132 ± 15
90201	L5	3.48 ± 0.07	2.38 ± 0.07	12.7 ± 0.3	8.4 ± 0.6	3.79 ± 0.11	0.66 ± 0.05	133 ± 23	124 ± 23	129 ± 16
93050	LL4	2.72 ± 0.12	1.86 ± 0.14	12.6 ± 0.3	–	4.75 ± 0.18	–	45 ± 26	–	*45 ± 26*[b]
97017	LL5	2.79 ± 0.07	1.89 ± 0.12	10.6 ± 0.2	8.0 ± 0.8	3.95 ± 0.11	0.75 ± 0.09	138 ± 22	102 ± 30	125 ± 18
93020	L5	2.36 ± 0.05	1.57 ± 0.04	9.1 ± 0.2	5.9 ± 0.8	4.02 ± 0.10	0.65 ± 0.08	145 ± 21	142 ± 33	144 ± 18
90205	L5	2.41 ± 0.05	1.58 ± 0.04	9.0 ± 0.2	6.4 ± 0.5	3.87 ± 0.12	0.72 ± 0.06	163 ± 23	120 ± 24	142 ± 22
94247	LL6	2.03 ± 0.10	1.3 ± 0.3	8.2 ± 0.2	–	4.21 ± 0.23	–	132 ± 34	–	132 ± 34
90218	L5	1.68 ± 0.04	1.06 ± 0.05	7.2 ± 0.2	5.5 ± 0.7	4.43 ± 0.16	0.76 ± 0.10	116 ± 26	109 ± 32	113 ± 20
97429	LL5	1.53 ± 0.04	1.34 ± 0.05	6.8 ± 0.2	4.9 ± 0.7	4.63 ± 0.15	0.72 ± 0.11	98 ± 24	124 ± 37	105 ± 20
90286	L5	1.60 ± 0.05	0.96 ± 0.03	6.2 ± 0.1	4.6 ± 0.6	4.03 ± 0.15	0.75 ± 0.09	169 ± 26	114 ± 32	147 ± 27
90207	L5	1.04 ± 0.02	0.71 ± 0.05	4.5 ± 0.1	3.7 ± 0.4	4.49 ± 0.14	0.82 ± 0.08	128 ± 23	96 ± 27	115 ± 18
971003	LL5	0.97 ± 0.03	0.64 ± 0.04	4.3 ± 0.1	3.1 ± 0.3	4.64 ± 0.15	0.73 ± 0.07	113 ± 24	124 ± 26	118 ± 18
Other QUE chondrites										
93021	L5	3.36 ± 0.07	2.91 ± 0.10	17.5 ± 0.3	17.9 ± 0.9	5.26 ± 0.12	1.02 ± 0.05	–	20 ± 18	20 ± 18
97013	LL5	5.57 ± 0.12	4.00 ± 0.20	19.7 ± 0.3	16.1 ± 1.7	3.68 ± 0.10	0.82 ± 0.09	61 ± 22	53 ± 29	58 ± 17
97028	LL5	5.47 ± 0.15	–	20.5 ± 0.4	–	3.98 ± 0.11	–	64 ± 23	–	64 ± 23

[a]The ^{36}Cl/^{10}Be ratios were normalized to H-chondrite metal composition, based on the measured Ni concentration in the metal, using a correction factor of (1 + 0.0025*[Ni-9]). Terrestrial ages (T36 and T41, in kyr) were derived from the ratios of ^{36}Cl/^{10}Be and ^{41}Ca/^{36}Cl in the metal phase (see text).
[b]The terrestrial age for QUE 93050 (in italics) was not included in calculating the average terrestrial age of the QUE 90201 shower.

Table 3. Measured concentrations of major elements (in wt%) and cosmogenic radionuclides (in dpm kg^{-1}) in stone fraction of 13 probable members of the QUE 90201 shower.

QUE	Type	Mg	Al	K	Ca	Mn	Fe	Ni	Depth	^{10}Be	^{26}Al	^{36}Cl	^{41}Ca
97998	LL5	16.4	1.27	0.094	1.34	0.28	17.4	0.08	4	18.2 ± 0.4	49.8 ± 1.1	5.7 ± 0.1	4.8 ± 0.3
97463	LL5	16.1	1.27	0.089	1.34	0.28	18.3	0.10	9	17.6 ± 0.4	51.9 ± 1.2	6.0 ± 0.1	5.4 ± 0.3
90201	L5	15.0	1.28	0.095	1.40	0.30	16.0	0.06	11	18.5 ± 0.4	48.9 ± 1.0	5.0 ± 0.1	6.0 ± 0.4
93050	LL4	16.7	1.22	0.084	1.55	0.25	18.5	0.61	11	16.8 ± 0.3	52.5 ± 1.6	5.8 ± 0.1	–
97017	LL5	15.7	1.38	0.099	1.38	0.31	15.7	0.06	25	16.2 ± 0.3	47.0 ± 1.6	4.9 ± 0.1	7.1 ± 0.5
93020	L5	15.4	1.31	0.097	1.51	0.31	17.5	0.21	35	15.1 ± 0.3	48.3 ± 1.2	4.8 ± 0.1	13.7 ± 0.7
90205	L5	15.2	1.34	0.094	1.52	0.32	16.7	0.10	37	14.0 ± 0.3	43.1 ± 1.0	4.4 ± 0.1	7.2 ± 0.4
94247	LL6	–	1.32	0.085	1.66	0.26	17.7	0.39	44	14.3 ± 0.3	46.0 ± 1.4	5.0 ± 0.1	–
90218	L5	14.9	1.35	0.097	1.48	0.31	18.6	0.24	55	11.4 ± 0.2	35.7 ± 0.9	4.0 ± 0.1	12.7 ± 0.6
97429	LL5	16.5	1.23	0.092	1.46	0.28	18.6	0.16	59	11.7 ± 0.4	37.2 ± 0.8	4.2 ± 0.1	14.7 ± 0.7
90286	L5	15.2	1.26	0.098	1.30	–	17.8	0.28	67	11.2 ± 0.2	34.9 ± 1.0	3.7 ± 0.1	10.5 ± 0.5
90207	L5	14.3	1.28	0.096	1.71	0.30	17.5	0.14	96	8.1 ± 0.2	27.7 ± 0.7	2.9 ± 0.1	15.3 ± 0.7
971003	LL5	16.3	1.26	0.094	1.33	0.28	17.2	0.07	100	7.9 ± 0.2	25.2 ± 0.5	2.4 ± 0.1	11.9 ± 0.9

Note: Depth estimates (in cm) are from Fig. 6b.

avoid interlaboratory bias. Concentrations (in atoms g^{-1}) were converted to activities (in dpm kg^{-1}) by adopting half-lives of 1.36 Myr for ^{10}Be (Nishiizumi et al. 2007), 0.705 Myr for ^{26}Al (Nishiizumi 2004), 0.301 Myr for ^{36}Cl (Sharma et al. 1990), and 0.104 Myr for ^{41}Ca (Nishiizumi et al. 2000). The results given in Tables 2 and 3 include all known uncertainties (1σ) in the AMS measurements of the samples, standards, and blanks, but not the uncertainties in the absolute values of the AMS standards (or in the half-lives). For cosmogenic radionuclide concentrations in meteorites, which are reported as activities (in dpm kg^{-1}), the absolute uncertainties in the isotopic ratios of the AMS standards are irrelevant, whereas the absolute uncertainties in the activity of the standards are typically 1–2%. Concentrations of ^{10}Be and ^{26}Al in the metal fraction were corrected for small contributions of ^{10}Be and ^{26}Al from silicate contamination. The amount of silicate contamination in the metal was estimated from the concentration of Mg in the dissolved metal sample (Table 1), assuming an average Mg concentration of 17 wt% in the silicates. Corrections were made based on the measured concentrations of ^{10}Be and ^{26}Al in the stone fraction (Table 3).

Electron Microprobe Analysis

As the reported olivine-Fa and pyroxene-Fs compositions of many L5 chondrites from the QUE 90xxx and 93xxx collections are on the high end of the L chondrite range, olivine and pyroxene compositions of six L5 chondrites (QUE 90201, 90205, 90207, 90218, 93020, and 93021) were determined using a JEOL JXA 8900R electron microprobe at the Smithsonian Institution operated with a 15 keV accelerating potential and 20 nA beam current, using well-known standards and manufacturer-supplied data reduction software. The calibration was verified with the Springwater (pallasite) olivine standard, which gave very consistent values near its ideal composition of 17.6 mole% fayalite (Fa).

Model Calculations

We calculated production rates of cosmogenic radionuclides in the stone and metal fraction of spherical objects with L chondrite composition and radii of 1–2 m. Particle fluxes are based on the LCS model, which combines the LAHET Code System for interactions of charged particles and neutrons above 20 MeV and the Monte Carlo N-Particle code for low-energy neutrons (Masarik and Reedy 1994a; Masarik et al. 2001). For typical meteoroid orbits in the main asteroid belt between 2 and 3 AU, we assumed an effective flux of primary galactic cosmic-ray particles of 4.8 protons cm^{-2} s^{-1} for energies above 10 MeV. We used previously evaluated cross sections for proton- and neutron-induced reactions, which were able to reproduce the measured cosmogenic nuclide depth profiles in lunar samples (Reedy and Arnold 1972) and in several meteorites, such as Knyahinya (Reedy et al. 1993). The production rates from the LCS model are identical to those previously used for deriving the preatmospheric size of the large Gold Basin L chondrite shower (Welten et al. 2003) and the Frontier Mountain (FRO) 90174 H chondrite shower (Welten et al. 2010a). More recent model calculations by Leya and Masarik (2009) use the same particle transport codes, but a slightly different set of neutron cross sections.

In addition to the purely physical models of Masarik and Reedy (1994a) and Leya and Masarik (2009), we also calculated production rates of ^{10}Be and ^{26}Al in stone and metal fractions using the

semiempirical model of Honda et al. (2002) for objects with radii of 85–225 cm. A more detailed description of the parameters used in the Honda model can be found in Honda et al. (2002) and Welten et al. (2003). A detailed cosmogenic nuclide record of the large Gold Basin L chondrite revealed that the semiempirical model of Honda yields more reliable ^{10}Be and ^{26}Al production rates for very large objects, while the purely physical model of Masarik and Reedy (1994a, 1994b) yields more reliable neutron-capture ^{41}Ca production rates (Welten et al. 2010a).

MINERAL COMPOSITION AND CLASSIFICATION

Metal Composition and Classification

Although the metal composition is not routinely used for the classification of ordinary chondrites, it is well known that the concentrations of Ni, Co, and other siderophile elements in the bulk metal vary systematically between H, L, and LL chondrite falls (Rambaldi 1976, 1977; Kong and Ebihara 1997). Figure 2 shows that many of the QUE L5 chondrites have lower bulk metal contents than L chondrite falls, which typically contain 7–10 wt% metal (Jarosewich 1990). The low metal contents of six L5 chondrites (QUE 90201, 90205, 90207, 90218, 90286, and 93020) coincide with high Ni and Co concentrations in the metal, which fall in the low end of the LL chondrite range (20–70 wt% Ni, 1.0–3.5 wt% Co). The fresh appearance of these L5 chondrites, which were all assigned to weathering category A/B, suggests that the low metal contents are not due to weathering. In addition, the measured Ni/Co ratios of approximately 21 in the metal are typical for chondritic metal and argue against the possibility that the high Ni concentrations in the metal are an artifact of HF leaching, which preferentially dissolves kamacite, thus increasing the Ni/Co ratio of the remaining metal. We thus conclude that the low bulk metal content (4 ± 1 wt%) as well as the metal composition of these six L5 chondrites is more consistent with classification as LL chondrites. This could suggest that these meteorites were either misclassified or belong to an intermediate group of L/LL chondrites, which have properties both of L and LL chondrites (Rubin 1990). Interestingly, the metal compositions in these six L5 chondrites, which belong to the QUE 90201 L5 chondrite shower, overlap with those of five LL5 chondrites (QUE 97017, 97429, 97463, 97998, and 971003) analyzed in this study. In total, 11 chondrites classified as L5 or LL5 have similar metal compositions, with an average of 24.8 ± 1.3 wt% Ni and 1.20 ± 0.12 wt% Co. This constant metal composition—relative to the wide range of 12–70 wt% Ni and 0.6–3.5 wt% Co observed for L and LL chondrite falls—is consistent with the hypothesis that these L5 and LL5 chondrites came from the same preatmospheric object, but additional evidence (such as cosmogenic nuclide concentrations) is needed to verify this hypothesis.

By contrast, the metal compositions of the L5 chondrite QUE 93021, and the LL5 chondrites QUE 97013 and 97028 are distinct from that of the QUE 90201 group (Fig. 2). The Ni and Co concentrations in the metal fraction of QUE 93021 are at the low end of the L chondrite range, consistent with its classification as L5, whereas Ni and Co concentrations in QUE 97028 metal are in the middle of the LL chondrite range, but significantly higher than those of the QUE 90201 group. Note that QUE 97028 falls on the left of the main LL chondrite trend, suggesting that metal separation was not complete for this sample. The measured metal composition of QUE 97013 was affected by (excessive) HF leaching, which dissolved more than 50% of the metal; extrapolation to its original composition suggests that QUE 97013 may be an L chondrite, consistent with its relatively high metal content of approximately 7 wt%.

Finally, the metal fractions of seven other chondrites classified either as L5 (QUE 93182, 97022, 97039, 97047, 99010, and 99013) or LL5 (QUE 99017) have Ni contents of approximately 10 wt% and Co contents of approximately 0.5 wt%, in the range typical of H chondrite metal (Rambaldi 1976). These results were reported in the Antarctic Meteorite Newsletter, along with the conclusion that these meteorites should be reclassified as H chondrites (Welten and Nishiizumi 2007). These meteorites will not further be discussed in this article, as they are clearly not linked to the QUE 90201 shower.

Silicate Composition and Classification

Because of the uncertainty in classification of some of the QUE L5 chondrites, we re-examined the olivine and pyroxene compositions of the L5 chondrites QUE 90201, 90205, 90207, 90218, and 93020. The olivine compositions in these L5 chondrites with low bulk metal and high metal-Ni concentrations, show a very tight range of 26.7–27.2 mole% Fa, which is essentially identical to the original values of Mason (26–27 mole% Fa) and intermediate between L chondrites (22.7–25.6 mole%) and LL chondrites (27.5–30.2 mole%) (Gomes and Keil 1980), although others might classify them as LL chondrites (Rubin 1990; Brearley and Jones 1998). The pyroxene-Fs compositions

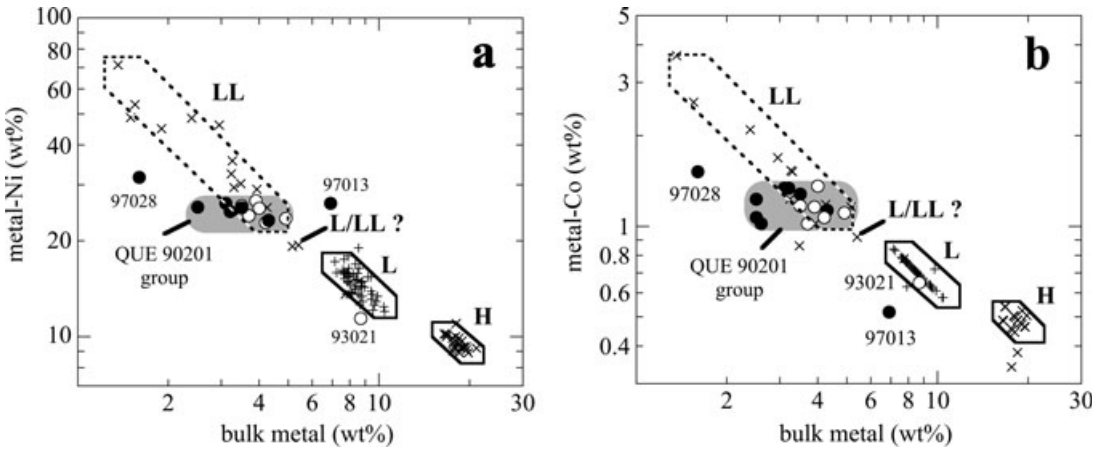

Fig. 2. Concentrations of a) Ni and b) Co in bulk metal of QUE L chondrites (open circles) and LL chondrites (closed circles) versus literature data (crosses) for ordinary chondrite falls (Jarosewich 1990). Shaded area indicates relative constant composition for QUE L5 and LL5 chondrites belonging to the QUE 90201 shower.

(22.1–22.4 mole%) are either on the high end of the L chondrite range (18.7–22.6 mole%; Gomes and Keil 1980), or the low end of the LL chondrite range (22–26 mole%; Brearley and Jones 1998). However, the relatively high CaO concentrations in low-Ca pyroxene (1.8–2.0 mole% Wo) seem to favor classification as L chondrites (Brearley and Jones 1998). It thus seems that these meteorites have properties of both L and LL chondrites. These observations confirm those of several other authors (e.g., Rubin 1990; Mason, personal communication), who have suggested that the hiatus between L and LL chondrites may not be as distinct as originally suggested by Keil and Fredriksson (1964). Rubin (1990) designated such meteorites with intermediate compositions as L/LL, although it remains controversial whether these meteorites sample a distinct parent body. Although one of the authors (K. C. W.) favors classification of QUE 90201, 90205, 90207, 90218, 90286, and 93020 as LL chondrites—based on the metal content and composition—we propose that classification as L/LL5 chondrites is probably most accurate. It may be interesting to investigate the heterogeneity of the silicates in these QUE L/LL5 chondrites in more detail by oxygen isotope analysis to further investigate the distinction between L and LL chondrites and/or the viability of a separate L/LL chondrite subgroup (Rubin 1990; Ahn et al. 2009).

TERRESTRIAL AGE

In the past, terrestrial ages of Antarctic chondrites were mostly determined from the concentration of cosmogenic ^{14}C in bulk samples for meteorites younger than 40 kyr (Jull 2001) and/or from ^{36}Cl or ^{41}Ca in the metal phase for meteorites older than 40 kyr (Nishiizumi et al. 1989a; Klein et al. 1991a). The latter methods are based on a relatively constant production rates of 22.1 ± 2.8 dpm kg^{-1} for ^{36}Cl (Nishiizumi et al. 1989a) and 24 ± 1 dpm kg^{-1} for ^{41}Ca (Klein et al. 1991a). These values are valid for >90% of the Antarctic chondrites, as they generally represent objects with preatmospheric radii <50 cm. However, for larger objects, the production rates of ^{36}Cl and ^{41}Ca (as well as other radionuclides) are significantly lower than the average saturation values, as was shown for several large chondrite showers, including FRO 90174 (Welten et al. 2001a) and Gold Basin (Welten et al. 2003). The simple calculation of terrestrial ages from ^{36}Cl and ^{41}Ca concentrations in large chondrites may lead to large discrepancies between the ^{36}Cl and ^{41}Ca ages. This is clearly the case for the QUE L5 and LL5 chondrites, which show apparent terrestrial ages up to 700 kyr based on ^{36}Cl and ages up to 300 kyr based on ^{41}Ca. We therefore calculated terrestrial ages using shielding-corrected methods based on the $^{36}Cl/^{10}Be$ and $^{41}Ca/^{36}Cl$ ratios (see Appendix).

Despite large variations in the concentrations of ^{10}Be, ^{36}Cl, and ^{41}Ca in the metal phase, the $^{36}Cl/^{10}Be$ and $^{41}Ca/^{36}Cl$ ratios in 12 out of 16 of the QUE L5 and LL5 chondrites are relatively constant (Fig. 3). The ratios correspond to terrestrial ages of 100–160 kyr based on the $^{36}Cl/^{10}Be$-^{10}Be method ratios and ages of 90–150 kyr based on the $^{41}Ca/^{36}Cl$-^{36}Cl method. The overlapping terrestrial ages confirm our hypothesis that most of these L and LL chondrites originated from a single large object in which shielding attenuated the production rates of cosmogenic nuclides. We will refer to these meteorites as the QUE 90201 shower. One sample, QUE 93050 (LL4), shows similarly low ^{10}Be, ^{26}Al, and ^{36}Cl concentrations, but its $^{36}Cl/^{10}Be$ ratio falls approximately 20% above the ratios of the other QUE 90201 chondrites, thus leading to a much younger terrestrial age of approximately 45 kyr

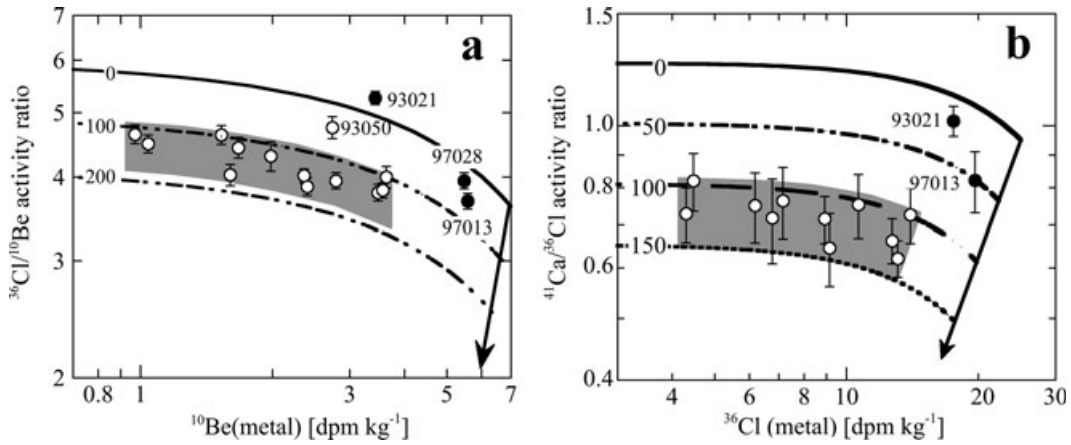

Fig. 3. Measured activity ratios of a) ^{36}Cl/^{10}Be and b) ^{41}Ca/^{36}Cl ratios in the metal phase of QUE L5 and LL5 chondrites versus measured concentrations of ^{10}Be and ^{36}Cl in the metal phase. Open symbols represent samples belonging to the QUE 90201 shower, closed symbols represent two or three distinct falls, QUE 93021, 97013, and 97028. The solid curves (labeled "0") correspond to the empirical correlations for falls (Equations A1 and A2), whereas the dashed curves correspond to terrestrial ages of 100 and 200 kyr in panel (a) and 50, 100, and 150 kyr in panel (b). The shaded areas include all samples that belong to the QUE 90201 shower, highlighting the correlation between ^{36}Cl/^{10}Be versus ^{10}Be and ^{41}Ca/^{36}Cl versus ^{36}Cl for the QUE L/LL5 chondrites. The elevated ^{36}Cl/^{10}Be ratio in QUE 93050 is discussed in the text. No ^{41}Ca data are available for QUE 93050 and 97028.

(Table 2). Based on the ^{10}Be, ^{26}Al, and ^{36}Cl concentrations in the stone fraction of QUE 93050, which also overlap with those of the QUE 90201 chondrites, we assume that this sample is also part of the QUE 90201 shower. The elevated ^{36}Cl/^{10}Be ratio in QUE 93050 can be due to a high ^{36}Cl or a low ^{10}Be concentration in the metal fraction. While the ^{10}Be and ^{26}Al concentrations in this sample suggest that it experienced similar shielding as QUE 97017, the ^{36}Cl concentrations (in metal and stone) suggest that QUE 93050 was closer to the preatmospheric surface, i.e., similar to QUE 90201, 97463, and 97998. A possible (but somewhat speculative) explanation for the elevated ^{36}Cl/^{10}Be ratio in QUE 93050 could be that a small chunk of the QUE 90201 meteoroid was knocked off in the last approximately 0.5 Myr, thus bringing QUE 93050 closer to the surface of the meteoroid, leading to a higher ^{36}Cl production rate. This scenario is similar to the one proposed for two samples of the large NWA 869 shower, which also show elevated ^{36}Cl/^{10}Be ratios in the metal (Welten et al. 2010b).

The remaining three QUE L5 or LL5 chondrites (QUE 93021, 97013, and 97028) show significantly higher ^{36}Cl concentrations of 17.5–20.5 dpm kg^{-1}, corresponding to terrestrial ages <80 kyr. In addition, the ^{10}Be concentrations of approximately 5.5 dpm kg^{-1} (metal) in QUE 97013 and 97028 are much higher than those in the QUE 90201 shower, indicating much lower shielding conditions, most likely in an object <30 cm in radius. These two meteorites may be paired, as is also supported by their almost identical NTL values of approximately 41 krad (Benoit et al. 2000). Although the ^{10}Be concentration in the metal phase of QUE 93021 is within the range of the QUE 90201 meteorites, the ^{36}Cl and ^{41}Ca concentrations are much higher, indicating a short terrestrial age (<40 kyr). In addition, the ^{36}Cl/^{10}Be ratios are above the curve that is observed for falls, indicating QUE 93021 had a short CRE age (<5 Myr), which is supported by the high ^{26}Al/^{10}Be ratio in the metal fraction.

The distribution of the QUE L5 and LL5 chondrites on the ice does not show a typical meteorite strewn field pattern, but is scattered all over the QUE meteorite stranding site, covering an area of > 50 km^2. The lack of a typical strewn field pattern is not surprising for Antarctic meteorite showers, as most of the meteorite fragments were moved from their original location of fall due to transport of meteorites within the ice and/or redistribution of small meteorites by eolian transport on the ice. To exclude the possibility that these specimens represent two (or more) overlapping showers, we will compare the measured radionuclide concentration in both the metal and stone phase with calculated depth profiles of cosmogenic nuclide production rates, based on Masarik and Reedy (1994a), Honda et al. (2002), and Leya and Masarik (2009).

PREATMOSPHERIC SIZE AND DEPTH

Large meteorites (R > 1 m) are characterized by large variations in the concentrations of cosmogenic radionuclides as a function of depth (Welten et al. 2003, 2010a). The most clear indications of a large preatmospheric size are low concentrations of spallogenic nuclides (^{10}Be, ^{26}Al, ^{36}Cl, and ^{41}Ca) in the metal fraction,

high ^{10}Be(stone)/^{10}Be(metal) and ^{26}Al(stone)/^{26}Al(metal) ratios, and high concentrations of neutron-capture produced nuclides (^{36}Cl and ^{41}Ca) in the stone fraction. To verify that the QUE 90201 samples represent a single preatmospheric object, and to constrain the size of this object, we compare the radionuclide concentrations in both the metal and stone fractions in the QUE samples with calculated production rates (and ratios) for large objects. To do so, we converted the measured radionuclide concentrations to those at the time of fall, by correcting for radioactive decay during their terrestrial residence time of 125 ± 25 kyr. Corrections factors are 1.066 ± 0.014 for ^{10}Be, 1.13 ± 0.03 for ^{26}Al, 1.33 ± 0.08 for ^{36}Cl, and 2.3 ± 0.4 for ^{41}Ca.

Production Rates of Spallogenic Nuclides

To constrain the preatmospheric size of the QUE 90201 object, we will compare measured saturation values of cosmogenic radionuclides that are exclusively formed by medium to high-energy spallogenic reactions (at energies of > 10 MeV), including ^{10}Be and ^{36}Cl in the metal phase and ^{10}Be and ^{26}Al in the stone phase, with calculated production rates. As the production rate ratios of ^{26}Al/^{10}Be and ^{41}Ca/^{36}Cl in the metal fraction are relatively constant at ~0.7 and ~1.1, respectively, we will not discuss the ^{26}Al and ^{41}Ca concentrations in the metal phase, as these would yield the same conclusions as those derived from ^{10}Be and ^{36}Cl in the metal, respectively.

The radionuclide saturation values in the metal phase of the QUE 90201 shower vary by a factor of 3–4, from 1.0 to 3.9 dpm kg^{-1} for ^{10}Be and 5.7–18.5 dpm kg^{-1} for ^{36}Cl, respectively. Model calculations show that a minimum radius of approximately 120 cm is required to cause a factor of 3–4 variation in the ^{10}Be and ^{36}Cl production rates in the metal phase as a function of depth in a single object. On the other hand, a radius > 2 m is difficult to reconcile with the relatively high concentrations of ^{10}Be (~18 dpm kg^{-1}) and ^{26}Al (~50 dpm kg^{-1}) in the stone fraction of the least shielded samples, notably QUE 90201, 97463, 97998. These simple observations suggest that the QUE 90201 meteoroid had a radius in the range of 120–200 cm.

We can further constrain the size of the preatmospheric object by combining the ^{10}Be and ^{26}Al saturation concentrations in the metal and stone fractions of the QUE 90201 shower, as we previously did for the FRO 90174 shower (R = 80–100 cm; Welten et al. 2001a) and the Gold Basin shower (R = 3–5 m; Welten et al. 2003). The combined ^{10}Be and ^{26}Al concentrations in QUE 90201 indicate a preatmospheric radius larger than that of FRO 90174 (i.e., > 1 m), which showed relatively constant ^{10}Be and ^{26}Al concentrations in the stone fraction, but smaller than that of the Gold Basin meteoroid (i.e., <3 m), which showed much larger variations of ^{10}Be and ^{26}Al in the stone and metal fractions than those observed in the QUE 90201 shower. Although none of the calculated radionuclide depth profiles for objects with radii between 85 cm and 3 m is a perfect match to the measured ^{10}Be and ^{26}Al concentrations in the stone and metal fraction of the QUE 90201 shower, a radius of approximately 150 cm provides the best match with the ^{10}Be and ^{26}Al data, as shown in Fig. 4. Of the three models, the semiempirical model (Honda et al. 2002) yields the best agreement with the measured ^{10}Be and ^{26}Al concentrations, whereas the model of Leya and Masarik (2009) shows the largest discrepancies. In general, the differences between the three model calculations are larger for ^{10}Be than they are for ^{26}Al.

Two additional shielding indicators are the ratios of ^{10}Be(stone)/^{10}Be(metal) and ^{26}Al(stone)/^{26}Al(metal). As ^{10}Be and ^{26}Al in the *stone* fraction are mainly produced by secondary protons and neutrons, whereas ^{10}Be and ^{26}Al in the *metal* phase are mainly produced by primary cosmic-ray protons, the ratio of each nuclide in the stone over that in the metal fraction increases as a function of meteoroid size and depth (Nagai et al. 1993). The ^{10}Be(stone)/^{10}Be(metal) ratios in fragments of the QUE 90201 shower range from 5.0 to 8.2, and increase with decreasing ^{10}Be concentration in the metal (i.e., increasing depth), whereas the ^{26}Al(stone)/^{26}Al(metal) ratios increase from 20 to 40 (Fig. 5). The ratios are intermediate between those found in the FRO 90174 shower (Welten et al. 2001a) and in the much larger Gold Basin L chondrite shower (Welten et al. 2003). The ^{10}Be(stone)/^{10}Be(metal) and ^{26}Al(stone)/^{26}Al(metal) ratios thus confirm that the QUE 90201 meteoroid was intermediate in size between the FRO 90174 (R ~ 80 cm) and Gold Basin meteoroids (R = 3–5 m).

Adopting a preatmospheric radius of 150 cm for QUE 90201, we can derive the irradiation depth of each sample in the meteoroid by comparing the measured saturation values in fragments of the QUE 90201 shower with calculated production rates (Fig. 6). The saturation values of ^{10}Be (a) and ^{36}Cl (b) in the metal phase correspond to depths ranging from approximately 5 cm for the least shielded samples (QUE 90201, 97463, and 97998) to approximately 100 cm for the most shielded samples (QUE 90207 and 971003). On the other hand, the ^{10}Be (c) and ^{26}Al (d) concentrations in the stone fraction of the QUE 90201 shower seem to indicate 20–50% higher irradiation depths, up to 120–150 cm for the most shielded samples. Although some of the inconsistencies in the derived sample depth may be due to uncertainties of approximately 15% in the calculated cosmogenic nuclide production rates, we cannot exclude the possibility that

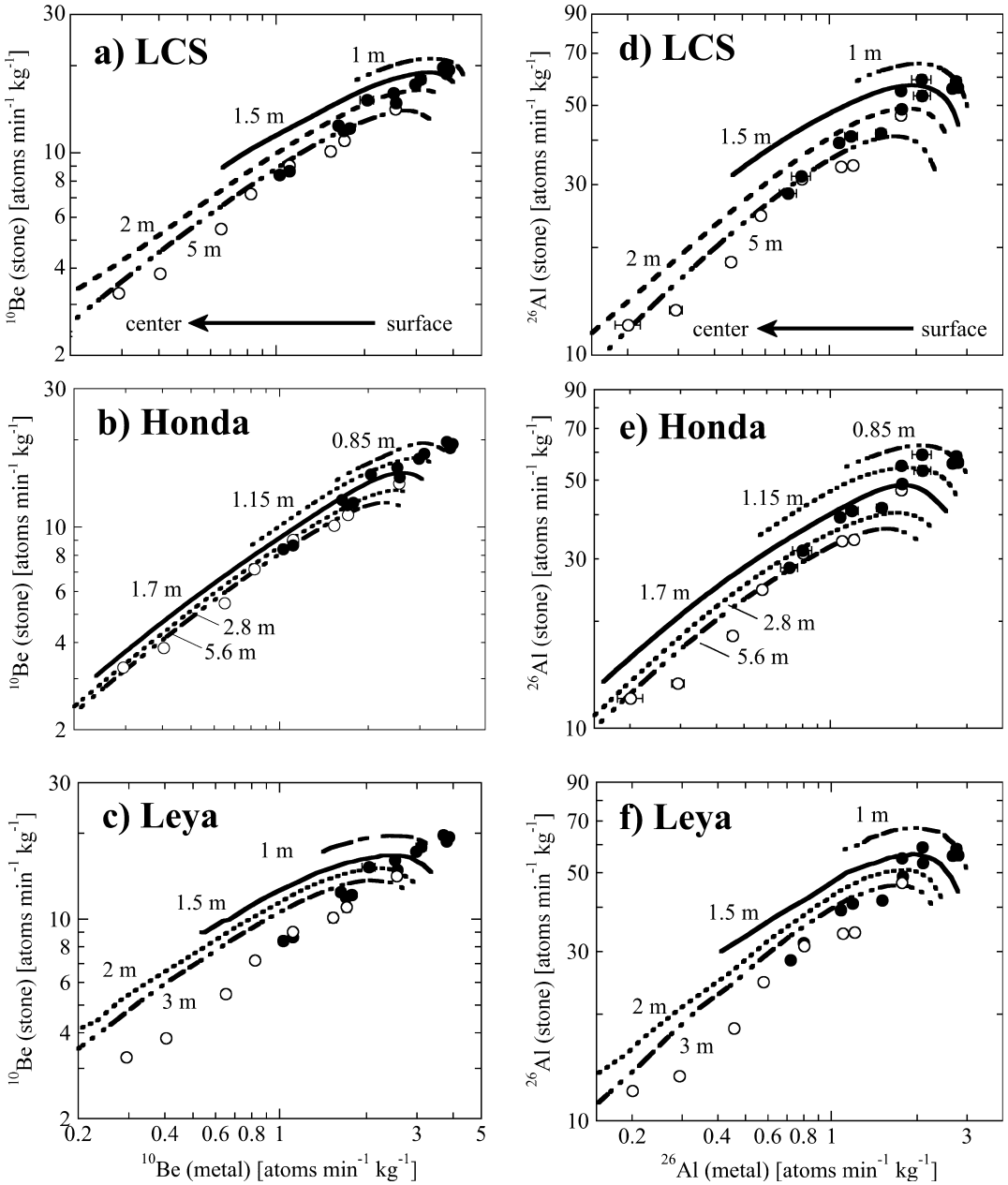

Fig. 4. Comparison of measured production rates of a–c) ^{10}Be and d–f) ^{26}Al in the metal and stone fractions of the QUE 90201 L/LL5 chondrite (solid symbols) and Gold Basin L4–6 chondrite shower (open symbols) with calculated production rates of ^{10}Be and ^{26}Al based on the Masarik and Reedy (1994a) model (top), the Honda et al. (2002) model (middle), and the Leya and Masarik (2009) model (bottom).

they are due to a nonspherical (e.g., ellipsoidal) shape of the QUE meteoroid, which tends to lower the production rates of low-energy products (^{10}Be in stone fraction) more than those of high-energy products (^{10}Be in metal) relative to spherical objects (Masarik and Reedy 1994b). The observed ^{10}Be(stone)/^{10}Be(metal) and ^{26}Al(stone)/^{26}Al(metal) ratios in QUE 90201 increase with shielding depth, as predicted by model calculations, but they are significantly lower than predicted by the models, as was previously also observed for Gold Basin (Welten et al. 2003, 2010a).

Neutron-Capture Production Rates

In large stone meteorites (R > 30 cm), a significant fraction of the secondary neutrons is slowed down to thermal energies (~0.03 eV). Due to the relatively high cross sections for capture of thermal neutrons by ^{35}Cl,

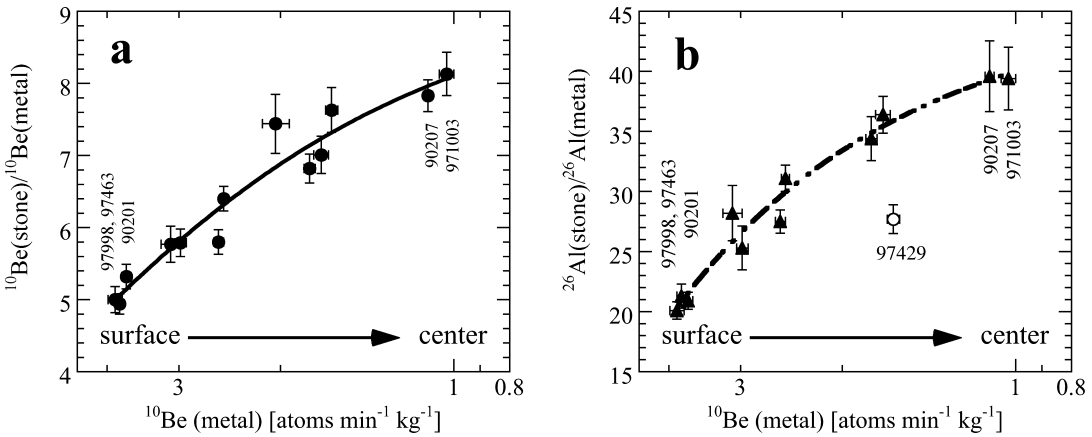

Fig. 5. Measured ratios of a) ^{10}Be(stone)/^{10}Be(metal) and b) ^{26}Al(stone)/^{26}Al(metal) in the QUE 90201 L/LL5 chondrite samples as a function ^{10}Be in the metal fraction, with the latter decreasing (from left to right) as a function of sample depth in a large meteoroid. Note that the relatively low ^{26}Al(stone)/^{26}Al(metal) ratio in one outlier (QUE 97429) is most likely due to the presence of ~0.3 wt% P in the metal (see Appendix).

^{40}Ca, and ^{59}Co, high fluxes of thermal neutrons in large chondrites result in significant production of neutron-capture ^{36}Cl, ^{41}Ca, and ^{60}Co. The thermal neutron fluxes reach a maximum in the center of stony meteoroids with a radius of approximately 300 g cm^{-2} (~85 cm) and show a steep increase from the surface to the center (Spergel et al. 1986). Neutron-capture products are thus a very sensitive measure of the preatmospheric size of a meteorite and depth of sample within the meteoroid. The radionuclide ^{60}Co is almost exclusively produced by neutron-capture, but due to its short half-life of 5.27 yr, it is generally only detected in meteorite falls and not in meteorite finds. The radionuclides ^{41}Ca and ^{36}Cl have much longer half-lives (1.04×10^5 and 3.01×10^5 yr, respectively) and are thus more suitable for studying neutron-capture reactions in stony meteorite finds (e.g., Bogard et al. 1995; Welten et al. 2001a, 2001b, 2003). However, these radionuclides are not only produced by neutron-capture reactions but also by spallation reactions, mainly on Ca and Fe for ^{36}Cl production and on Fe and Ni for ^{41}Ca production. In addition, the neutron-capture rates of ^{36}Cl and ^{41}Ca are dependent on the concentrations of the target elements, Cl and Ca. The concentration of Ca is relatively constant at approximately 1.5 wt% in the stone fraction of ordinary chondrites (Table 3), while Cl concentrations in ordinary chondrites vary from 5 to 200 ppm (Garrison et al. 2000) and are difficult to measure due to terrestrial contamination. We will therefore first discuss neutron-capture ^{41}Ca.

Neutron-Capture ^{41}Ca in the Stone Fraction

The measured ^{41}Ca concentrations in the stone fraction of QUE 90201 samples vary from 5 to 15 dpm kg^{-1} (Table 4). Unlike the concentrations of ^{10}Be and ^{26}Al in the stone fraction, which decrease with decreasing ^{10}Be concentrations in the metal phase, i.e., with increasing depth, those of ^{41}Ca increase a factor of approximately 3 with increasing depth (Fig. 7a). The different depth profile of ^{41}Ca relative to purely spallogenic nuclides is due to the production of ^{41}Ca from neutron-capture reactions on ^{40}Ca. From the measured concentrations of ^{41}Ca in the metal fraction (Table 2) and the concentrations of the major (Fe) and minor (Ti, Cr, and Mn) target elements in the stone fraction (Table 3), we estimate contributions of spallation produced ^{41}Ca in the stone fraction of 0.5–1.8 dpm kg^{-1}, i.e., 5–35% of the total ^{41}Ca content. This implies that the concentrations of ^{41}Ca in most QUE L/LL5 chondrites (Fig. 7a) are dominated by neutron-capture contributions, which increase from approximately 3 dpm kg^{-1} for the least shielded sample (QUE 97998) to approximately 14 dpm kg^{-1} for one of the most shielded samples (QUE 90207).

After normalizing the neutron-capture ^{41}Ca contributions in the stone fraction to the amount of Ca in each sample (typically 13–17 mg g^{-1}) and correcting for radioactive decay of ^{41}Ca (by a factor of 2.3) during the meteorite's terrestrial residence time, we find specific neutron-capture production rates ranging from 0.5 to 2.2 atoms min^{-1} g^{-1} Ca. The maximum values around approximately 2 atoms min^{-1} g^{-1} Ca in the QUE 90201 shower are similar to the maximum value found in Jilin (Klein et al. 1991b), but significantly higher than values of approximately 1.5 atoms min^{-1} g^{-1} Ca in several other large chondrites, such as Allende (Nishiizumi et al. 1991), Chico (Bogard et al. 1995), and FRO 90174 (Welten et al. 2001a). An interesting feature is that six of the most shielded QUE samples show a relatively constant neutron-capture ^{41}Ca production rate of 1.9 ± 0.2 atoms min^{-1} g^{-1} Ca, while ^{10}Be and ^{36}Cl

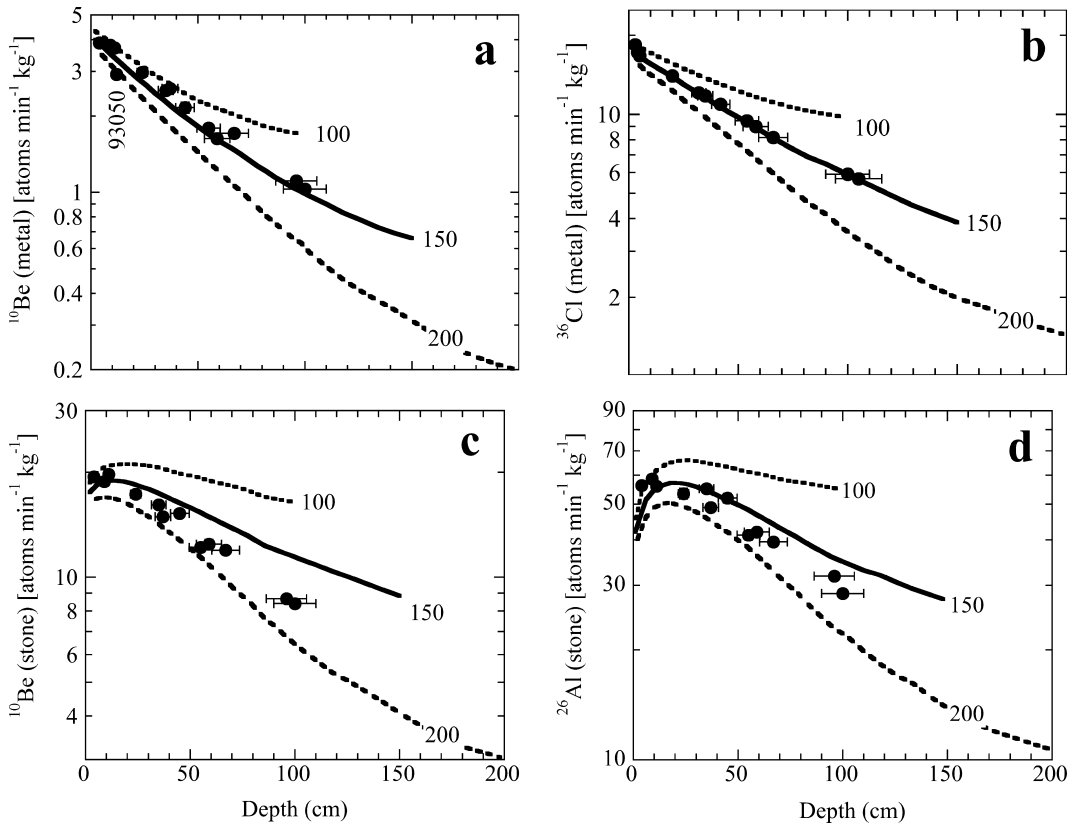

Fig. 6. Comparison of measured saturation values of ^{10}Be (a) and ^{36}Cl (b) in the metal fraction and ^{10}Be (c) and ^{26}Al (d) in the stone fraction of QUE L5 and LL5 chondrites with calculated production rates of ^{10}Be, ^{26}Al, and ^{36}Cl as a function of depth in chondritic objects of 100, 150, and 200 cm in radius using the LCS model. We estimated the irradiation depth for each sample by comparison of the measured ^{10}Be and ^{36}Cl concentrations in the metal phase of each sample with calculated ^{10}Be and ^{36}Cl depth profiles (a, b) and used the average depth estimates from the metal phase for figures (c) and (d).

concentrations in the metal phase indicate that these samples came from a wide range in shielding depths, which vary by >50 cm. Figure 7b shows that such a broad peak in the neutron-capture production rate is consistent with a preatmospheric radius of approximately 150 cm, confirming our size estimate based on spallogenic ^{10}Be, ^{26}Al, and ^{36}Cl concentrations.

Neutron-Capture ^{36}Cl in the Stone Fraction

In contrast to the concentrations of ^{41}Ca in the stone fraction, which show a factor of 3 increases with shielding depth, those of ^{36}Cl decrease almost a factor of 3 with shielding depth, from approximately 6 dpm kg^{-1} for the least shielded samples to approximately 2.3 dpm kg^{-1} for the most shielded samples (Fig. 8a). This implies that the production of ^{36}Cl in the stone fraction of the QUE 90201 fragments is dominated by spallation reactions on Fe and Ca, while contributions from neutron-capture on Cl are small or negligible (<1 dpm kg^{-1}). Considering the large contributions of neutron-capture ^{41}Ca in the QUE 90201 samples, the lack of neutron-capture ^{36}Cl cannot be explained by low thermal neutron fluxes, but must be due to low Cl concentrations. Based on neutron-capture cross sections of 44 barn for ^{35}Cl and 0.43 barn for ^{40}Ca, the observed saturation value of approximately 2 dpm g^{-1} Ca for neutron-capture ^{41}Ca corresponds to a saturation value of approximately 200 dpm g^{-1} Cl for neutron-capture ^{36}Cl. The observed neutron-capture ^{36}Cl contributions of <1 dpm kg^{-1} in the QUE 90201 shower therefore indicate Cl concentrations of <5 mg kg^{-1} (ppm). These inferred Cl concentrations are on the low end of the range of 5–200 ppm observed for ordinary chondrites (Garrison et al. 2000). Unfortunately, it is difficult to verify these low Cl concentrations, as Antarctic meteorites are often contaminated with terrestrial Cl (e.g., Langenauer and Krähenbühl 1993), but the observed ^{36}Cl and ^{41}Ca concentrations leave no other conclusion.

Production of ^{36}Cl from Fe and Ca in the Stone Fraction

The contributions of ^{36}Cl from high-energy spallation reactions on Fe (including minor contributions from Cr, Mn, and Ni) can be derived from ^{36}Cl

Table 4. Spallation (sp) contributions of ^{36}Cl from Fe and Ca as well as spallation and neutron-capture (nc) contributions of ^{41}Ca in stone fraction of members of QUE 90201 L/LL5 chondrite shower.

QUE	$^{10}Be(s)/^{10}Be(m)$	$P(^{36}Cl)_{Ca}/P(^{36}Cl)_{Fe}$[a]	^{36}Cl (dpm kg^{-1})	$^{36}Cl(Fe)$[b] (dpm kg^{-1})	$^{36}Cl(Ca)$[c] (dpm kg^{-1})	^{41}Ca (dpm kg^{-1})	$^{41}Ca(sp)$ (dpm kg^{-1})	$^{41}Ca(nc)$ (dpm kg^{-1})	$^{41}Ca(nc)$[d] (atoms min^{-1} g^{-1} Ca)
97998	5.0 ± 0.2	14.4	5.7 ± 0.1	2.7 ± 0.1	3.3 ± 0.3	4.8 ± 0.3	1.75 ± 0.17	3.0 ± 0.4	0.50 ± 0.07
97463	5.1 ± 0.2	14.7	6.0 ± 0.1	2.6 ± 0.1	3.0 ± 0.3	5.2 ± 0.3	1.40 ± 0.09	3.8 ± 0.3	0.67 ± 0.07
90201	5.3 ± 0.2	15.3	5.0 ± 0.1	2.3 ± 0.1	3.3 ± 0.3	6.0 ± 0.4	1.37 ± 0.11	4.7 ± 0.4	0.75 ± 0.07
93050	–	16.5	5.8 ± 0.1	2.7 ± 0.1	3.8 ± 0.4	–	–	–	–
97017	5.6 ± 0.2	16.0	4.9 ± 0.1	1.9 ± 0.1	3.0 ± 0.3	7.1 ± 0.5	1.28 ± 0.14	5.8 ± 0.5	0.95 ± 0.09
93020	6.5 ± 0.2	18.5	4.8 ± 0.1	1.8 ± 0.1	3.0 ± 0.3	13.7 ± 0.7	1.02 ± 0.13	12.7 ± 0.7	1.92 ± 0.14
90205	5.8 ± 0.2	16.9	4.4 ± 0.1	1.7 ± 0.1	2.7 ± 0.3	7.2 ± 0.4	1.09 ± 0.09	6.1 ± 0.4	0.91 ± 0.08
94247	7.4 ± 0.4	20.1	5.0 ± 0.1	1.6 ± 0.1	3.3 ± 0.3	–	–	–	–
90218	7.1 ± 0.2	19.3	4.0 ± 0.1	1.5 ± 0.1	2.4 ± 0.2	12.7 ± 0.6	0.94 ± 0.12	11.7 ± 0.6	1.80 ± 0.13
97429	7.9 ± 0.3	21.0	4.2 ± 0.1	1.4 ± 0.1	2.4 ± 0.2	14.2 ± 0.7	0.84 ± 0.13	13.3 ± 0.7	2.16 ± 0.16
90286	7.1 ± 0.3	19.5	3.7 ± 0.1	1.3 ± 0.1	1.9 ± 0.2	10.5 ± 0.5	0.80 ± 0.10	9.7 ± 0.5	1.70 ± 0.13
90207	7.9 ± 0.2	21.1	2.9 ± 0.1	0.9 ± 0.1	1.9 ± 0.2	15.3 ± 0.8	0.64 ± 0.06	14.6 ± 0.8	1.96 ± 0.15
971003	8.2 ± 0.3	21.5	2.4 ± 0.1	0.9 ± 0.1	1.6 ± 0.2	12.5 ± 0.9	0.54 ± 0.05	11.9 ± 0.9	1.96 ± 0.17

[a] $P(^{36}Cl)_{Ca}/P(^{36}Cl)_{Fe} = 1.2*[27.6*\log\{^{10}Be(s)/^{10}Be(m)\} - 7.3]$.

[b] We included minor contributions from Cr, Mn, and Ni, assuming elemental ^{36}Cl production rates of 1.5, 1.2, and 0.8 times those for Fe.

[c] We included minor contributions from K and Ti, assuming elemental ^{36}Cl production rates of 2 and 0.5 times those for Ca, respectively.

[d] The specific neutron-capture ^{41}Ca saturation values (or production rates, in atoms min^{-1} g^{-1} Ca) are calculated by normalizing to the amount of Ca (Table 3) in each sample and correcting for radioactive decay of ^{41}Ca based on a terrestrial age of 125 kyr. The uncertainty in the terrestrial age is not included in the error, as all samples are affected in the same way. Note that the uncertainty in the terrestrial age would add an uncertainty of approximately 17% to the absolute production rates of neutron-capture ^{41}Ca given in the last column.

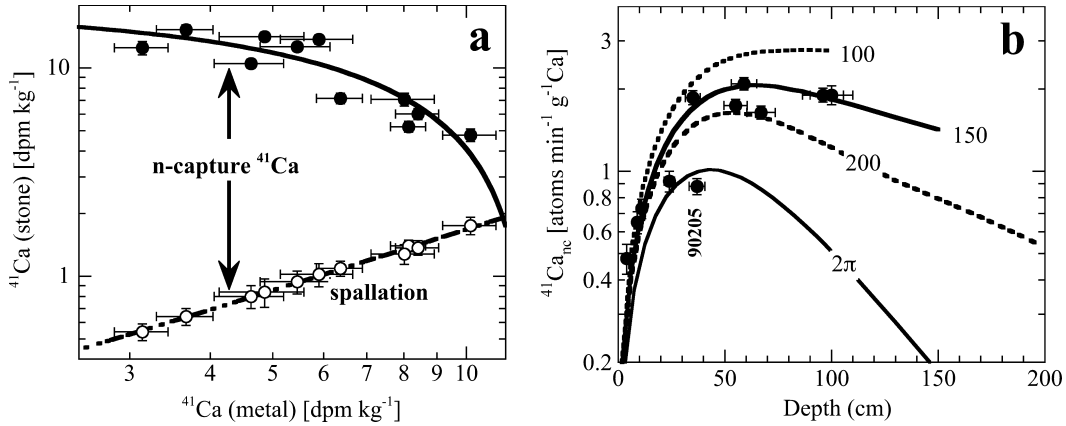

Fig. 7. Neutron-capture ^{41}Ca in stone fraction of QUE 90201. a) Measured ^{41}Ca concentrations (solid symbols) and estimated contributions of spallation produced ^{41}Ca (open symbols) in the stone fraction as a function of ^{41}Ca in the metal fraction; the difference between the two is the neutron-capture ^{41}Ca component. b) Neutron-capture ^{41}Ca contributions of QUE samples derived from panel (a), normalized to the amount of Ca and corrected for radioactive decay since time of fall, are compared to calculated production rates of neutron-capture ^{41}Ca as a function of depth in objects of 1–2 m in radius. The ^{41}Ca neutron-capture saturation values in most QUE samples (except QUE 90205) are consistent with irradiation in an object with a radius of approximately 150 cm, assuming the same irradiation depths that were previously derived from ^{10}Be and ^{36}Cl in the metal phase (Fig. 6).

concentrations measured in the metal phase combined with Fe concentrations measured in the stone phase (Table 4). Figure 8a shows that the contribution of ^{36}Cl from Fe decreases from approximately 50% of the total ^{36}Cl near the surface of QUE 90201 meteoroid to approximately 30% near the center. The remaining 50–70% of the total ^{36}Cl is mainly due to the production of ^{36}Cl from low-energy reactions on Ca and K (see Table 4). The good agreement between measured ^{36}Cl concentrations in the stone fraction and the estimated total spallation contributions from K, Ca and Fe confirm that neutron-capture ^{36}Cl contributions in the QUE 90201 samples are < 0.5 dpm/kg. While the production rate ratio, $P(^{36}Cl)_{Ca}/P(^{36}Cl)_{Fe} = 8$ for average sized meteorites (Nishiizumi et al. 1989b), it is known to be quite shielding dependent (e.g., Begemann et al. 1976; Welten et al. 2001a, 2001b; Leya and Masarik 2009). Our model calculations using LCS suggest that the $P(^{36}Cl)_{Ca}/P(^{36}Cl)_{Fe}$ ratio increases from approximately 9 near the surface of a 150 cm object to approximately 22 near the center, thus explaining the increase of the relative contribution of ^{36}Cl from Ca + K with depth as observed in Fig. 8a. Comparison of the measured ^{36}Cl saturation values with calculated production rates using the LCS model (Fig. 8b) shows relative good agreement for most samples, although the near-surface samples show a small excess of ^{36}Cl.

Preatmospheric Size and Shape

In conclusion, the combined cosmogenic radionuclide records in fragments of the QUE 90201 shower are consistent with a preatmospheric radius of approximately 150 cm, corresponding to a preatmospheric mass of approximately 50,000 kg. A meteoroid with a preatmospheric mass of 50,000 kg is the largest object among Antarctic stone meteorites identified to date. The only Antarctic meteorite similar in size to QUE 90201 is the Derrick Peak iron meteorite, which had a minimum preatmospheric mass of approximately 45,000 kg (Nishiizumi et al. 1987). The large size of QUE 90201 is—to our knowledge—surpassed by only a few non-Antarctic chondrites, including Tsarev (Nagai et al. 1993), Gold Basin (Welten et al. 2003), and NWA 869 (Metzler et al. 2008). Some of the discrepancies between measured cosmogenic radionuclide concentrations and calculated depth profiles may hint at a nonspherical shape of the QUE meteoroid.

MASS DISTRIBUTION OF QUE 90201 SHOWER

Mass Distribution and Degree of Pairing

Given the large preatmospheric size of the QUE 90201 object and the high percentage of L5 and LL5 chondrites with low natural TL levels in the QUE collection, it is plausible that the QUE 90201 shower includes the majority of the approximately 2100 QUE meteorites that are classified as L5 or LL5. The mass distribution of a meteorite collection site can provide clues on the presence of large showers if these showers dominate the collection (e.g., Huss 1991; Welten et al. 2006). Compared to the mass distribution of meteorites falling on Earth (Halliday et al. 1989), the QUE

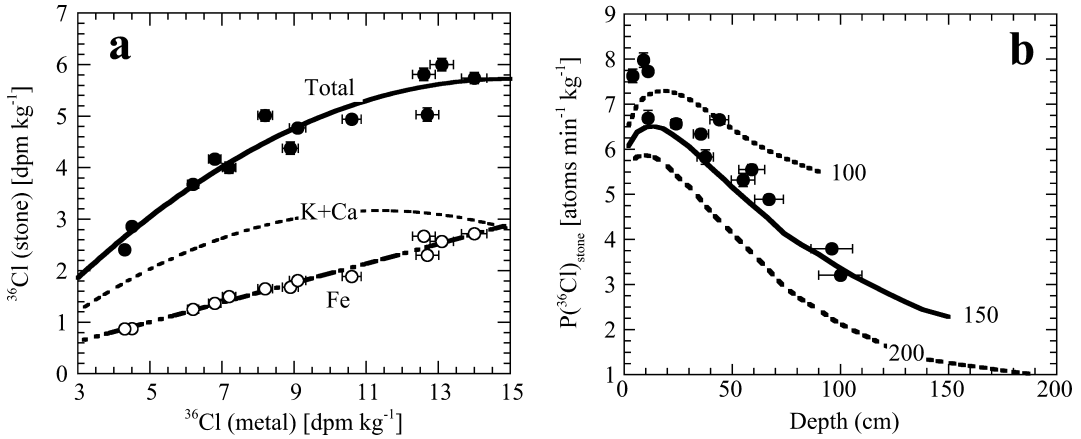

Fig. 8. Relationship of measured concentrations of ^{36}Cl in the stone fraction of QUE 90201 shower versus those of ^{36}Cl in the metal fraction (closed symbols in [a]). Open symbols and the semi-dashed line in (a) represent estimated contributions of ^{36}Cl from high-energy spallation on Fe, while the dashed curve labeled "K + Ca" represents estimated contributions of ^{36}Cl from low-energy spallation reactions on K + Ca and the solid curve represents the sum of the estimated spallation contribution from K + Ca and Fe (Table 4). Figure 9b shows comparison of measured ^{36}Cl concentrations (after correction by a factor of 1.33 due to radioactive decay since its fall 125 ka) with calculated ^{36}Cl production rate depth profiles in the stone fraction of chondritic objects with radii of 100–200 cm, using the LCS model. We used the same depth estimates for the QUE samples as in Fig. 6.

population shows a lack of meteorites >2 kg and a twofold excess of fragments <500 g (Fig. 9a). We conclude that this excess of small meteorites can almost entirely be attributed to the QUE 90201 L/LL5 chondrite shower. Note that only one of the five largest chondrites (>1 kg) classified as L5 or LL5 was confirmed as a member of the QUE 90201 shower, whereas QUE 93021 (2.1 kg) is an independent L5 chondrite fall and QUE 99010 and 99017 turned out to be H chondrites. Based on the close proximity of QUE 99016 and 99017, we assume that QUE 99016 (although not measured) is also an H chondrite and may be paired with QUE 99017. Therefore, the largest confirmed member of the QUE 90201 shower is QUE 90201 itself with a mass of approximately 1.28 kg, while 90% of the fragments are <80 g and 50% <9 g.

Figure 9 shows that the mass distribution of the QUE 90201 L/LL5 chondrites is different from that of the other QUE chondrites. The mass distribution of approximately 600 QUE H chondrites, for example, is very similar to the mass distribution of infalling meteorites as derived from fireball data (Halliday et al. 1989), indicating that the H chondrite collection at QUE is a representative sample of infalling meteorite masses. The L5 and LL5 chondrites clearly dominate the QUE collection in numbers, but represent "only" 25% of the total mass of meteorites recovered at QUE. Relative to other QUE meteorites and the average flux of meteorites to Earth, the L5 and LL5 chondrites show an excess of specimens <100 g and a lack of specimens >300 g. A similar excess of small specimens was also observed for the FRO meteorite collection, which shows an unusually large number of small H chondrites, resulting in an H/L chondrite ratio of approximately 4. Based on cosmogenic radionuclide measurements, Welten et al. (2006) concluded that the large number of small H chondrites at FRO was due to a large H3-6 chondrite shower. Similarly, based on the large number of small L5 and LL5 chondrites at QUE, combined with the high degree of pairing among L and LL chondrites investigated in this study, and the low natural TL levels in most of these samples, we estimate that >90% of the 2100 L5 and LL5 chondrite specimens are part of the QUE 90201 shower. We estimate that the total recovered mass of this shower is 65 ± 5 kg (Fig. 9b), which represents approximately 0.13% of the estimated preatmospheric mass of approximately 50,000 kg.

Mass Distribution and Atmospheric Fragmentation

The mass distribution does not only help in identifying the presence of large showers in meteorite collections, but may also provide information on the meteoroid's fragmentation process in the atmosphere. In general, a smooth mass distribution is believed to represent a single catastrophic fragmentation event, while humps in the mass distribution are interpreted to be the result of multiple fragmentation (Oddershedde et al. 1998). The latter paper also showed that the mass distributions of 16 meteorite showers show distinct scaling behavior over several orders of magnitude. The observed scaling exponents (β_0) can be compared to empirical exponents from laboratory fragmentation experiments to distinguish between single or multiple

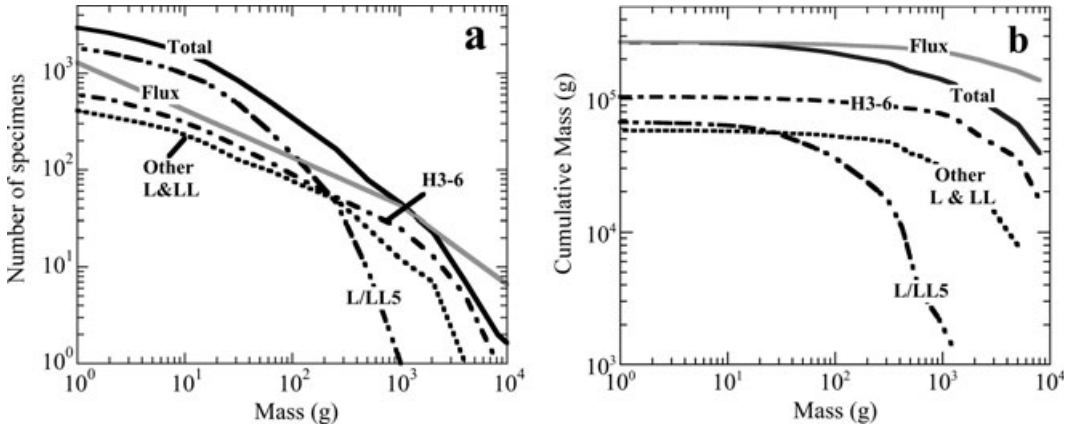

Fig. 9. Mass distribution of QUE meteorites plotted as a) cumulative number and b) cumulative mass versus recovered mass. The solid black curve represents all QUE meteorites, whereas the three dashed curves represent QUE H chondrites, QUE L/LL5 chondrites, and remaining L and LL chondrites. The gray curve represents the average influx of meteorites to Earth (Halliday et al. 1989) normalized to a total mass of 270 kg—equivalent to total mass of the QUE collection—and a largest mass of 70 kg, equivalent to the estimated total mass of the QUE 90201 shower, which represents the largest meteorite found at QUE (after correction for pairing).

fragmentation events and to derive the original shape of the meteoroid before entering the atmosphere.

Figure 10a shows the cumulative mass distribution of specimens >1 g for the QUE 90201 L/LL5 chondrite shower. The smooth mass distribution suggests that the QUE 90201 shower experienced a single fragmentation event. If we assume that all fragments >1 g were recovered, then the mass distribution of QUE 90201 yields $\beta_0 = 1.47 \pm 0.05$, with a characteristic cut-off mass of 210 g. However, as it seems unlikely that the recovery of meteorites with masses of 1–10 g is complete, we performed the same fitting procedure to the QUE mass distribution for masses above 10 g, which yields a slightly higher value of $\beta_0 = 1.58 \pm 0.06$. In simple fragmentation experiments (without atmospheric ablation), these scaling exponents are related to the shape of the meteoroid by an empirical equation, $\beta_0 = 1.1–0.21\ d_m + 0.13*(d_m)^2$, in which d_m is the dimensional measure, $d_m = 1 + 2\ (ab + ac + bc)/(a^2 + b^2 + c^2)$, where a, b, and c are the linear dimensions (axes) of the object. The L chondrite showers of Mbale (Jenniskens et al. 1994) and JaH 073 (Gnos et al. 2009) yield d_m values around 3, consistent with spherical objects (Oddershedde et al. 1998). Scaling exponents of 1.47 and 1.58 correspond to d_m values of 2.68–2.90. The low d_m values indicate an elongated shape for the QUE 90201 meteoroid in which—for example—the long axis was 1.5–2 times longer than the two short axes. This elongated shape is quite plausible considering recent evidence for the nonspherical shape of small asteroids such as 2008 TC_3, which impacted in the desert of northern Sudan in October 2008 (Scheirich et al. 2010).

Although the relatively low recovered mass of the QUE 90201 shower (<0.2% of the preatmospheric mass) may be partly due to incomplete recovery or loss of fragments on the ice, the mass distribution of QUE 90201 is quite different from that of the JaH 073 and Mbale showers (Fig. 10b), for which 10–20% of the preatmospheric mass survived atmospheric fragmentation. The different survival rates of these chondrite showers probably indicates differences in the atmospheric fragmentation process of these meteoroids as a function of preatmospheric size, physical strength, and/or entry velocity, as has been suggested by atmospheric fragmentation models (e.g., Hills and Goda 1993; Bland and Artemieva 2006). For example, model simulations of the atmospheric entry of meteoroids at typical entry velocities of 15–20 km s^{-1} suggest that typically 5–20% of the original mass survives atmospheric ablation (Bland and Artemieva 2006), while this value decreases to <1% for entry velocities of approximately 30 km s^{-1} or for very fragile objects. Interestingly, video observations of large fireballs (e.g., Nemtchinov et al. 1997; Borovicka and Kalenda 2003) suggest that most large meteoroids (>1000 kg) experience multiple fragmentation events in the atmosphere, resulting in much higher mass losses than from ablation alone. The observation that the large QUE 90201 meteoroid broke up into >2000 small fragments and lost more than 99% of its initial mass during atmospheric passage, is consistent with current models of catastrophic disruption of large meteoroids (at high altitude) in the atmosphere, and suggests that the QUE meteoroid was either much more fragile than the JaH 073 and Mbale L chondrite meteoroids or entered Earth's atmosphere at a higher velocity. The evidence that the catastrophic disruption of most large meteoroids like QUE 90201 involves multiple

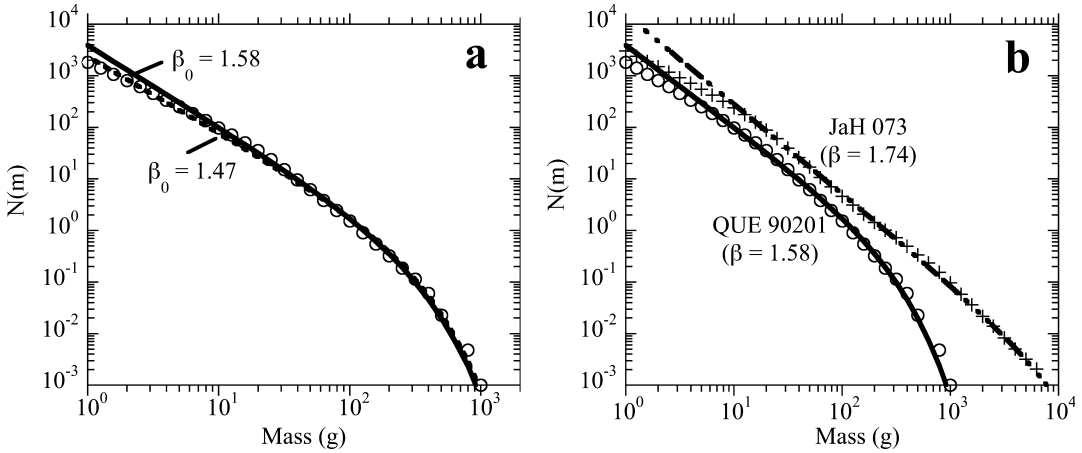

Fig. 10. a) Mass distribution, expressed as $N(m)$, of all 1830 fragments >1 g of the QUE 90201 L/LL chondrite shower. b) Comparison of QUE mass distribution with that of the L6 chondrite shower JaH 073. The JaH 073 shower consists of more than 3300 fragments with a total recovered mass of 600 kg (Gnos et al. 2009). The full and dashed curves in panel (a) represent exponential fits of $N(m) = C \exp(-m/m_0)\ m^{-\beta}$, based on the scaling analysis of Oddershedde et al. (1998), assuming complete recovery of all fragments >1 g (dashed curve) or >10 g (solid curve), respectively. The full and semi-dashed curves in panel (b) represent the exponential fits for the QUE 90201 and JaH 073 showers for fragments >10 g only.

fragmentation events contradicts the conclusion from the scaling analysis of the QUE 90201 shower. This contradiction questions the usefulness of scaling analysis of the mass distribution of large showers, which is based on fragmentation alone and does not take ablation effects into account. A similar conclusion was also reached for the Mbale meteorite shower (Rietmeijer and Nuth 2000), which clearly experienced multiple fragmentation events (Jenniskens et al. 1994), although the scaling analysis suggested a single event (Oddershedde et al. 1998).

Finally, the recent impact of the Carancas H chondrite, which produced a 14 m wide crater in Peru, showed that the atmospheric fragmentation process may be strongly dependent on entry velocity and angle, in addition to physical strength (Kenkmann et al. 2009). Knowledge of the preatmospheric size of large chondrite showers such as QUE 90201 and their mass distribution will provide ground truth for models of the atmospheric disruption of large stony objects upon their impact on Earth.

SUMMARY AND CONCLUSIONS

Cosmogenic radionuclide concentrations in the metal fractions of seven L5 and nine LL chondrites from the QUE stranding area indicate that 13 of these 16 chondrites (QUE 90201, 90205, 90207, 90218, 90286, 93020, 93050, 94247, 97017, 97429, 97463, 97998, and 971003) are part of a single large shower, QUE 90201. The members of this shower are characterized by (1) properties typical of L (pyroxene composition) and LL (e.g., metal abundance and composition) chondrites, as well as properties intermediate between the L and LL groups (e.g., olivine and pyroxene composition), suggesting that they are best described as L/LL5 chondrites; (2) large variations (factor of 3–4) in cosmogenic radionuclide concentrations in the metal phase; (3) relatively constant $^{26}Al/^{10}Be$, $^{36}Cl/^{10}Be$, and $^{41}Ca/^{36}Cl$ ratios in the metal phase consistent with a CRE age >5 Myr and an average terrestrial age of 125 ± 25 kyr; (4) large contributions of neutron-capture produced ^{41}Ca (0.5–2.1 dpm g^{-1} Ca at the time of fall) in the stone fraction; and (5) lack of neutron-capture produced ^{36}Cl, presumably due to very low Cl concentrations of <5 ppm.

Based on comparison of the measured concentrations of spallation and neutron-capture produced radionuclides with calculated depth profiles for an object with a radius of approximately 150 cm, we conclude that the samples came from shielding depths ranging from <5 to >100 cm. The fact that samples from very close to the preatmospheric surface survived atmospheric entry indicates that the meteoroid did not experience gradual ablation during atmospheric passage, but is consistent with catastrophic fragmentation. However, the agreement between model calculations and measurements is far from perfect. The calculated depth profiles show significant discrepancies with measured concentrations of cosmogenic radionuclides for the more shielded samples. Some of these discrepancies may be due to uncertainties in the model calculations. These uncertainties increase with increasing size of the object, where neutron induced reactions dominate production rates, while neutron cross sections have large uncertainties (up to a factor of ~2) due to

lack of empirical data. On the other hand, some of the discrepancies between measurements and model calculations may be due to a nonspherical shape of the meteoroid, as deviations between measurements and model seem to be larger than for the large Gold Basin meteoroid (Welten et al. 2003). Although an elongated shape of the meteoroid is supported by the scaling analysis of the mass distribution, the reliability of the scaling analysis of meteorite showers is questionable, as more than 99% of the original meteoroid mass of QUE 90201 was lost during atmospheric ablation, a process that is not taken into account in the scaling analysis.

The preatmospheric radius of 150 cm for the QUE 90201 shower is equivalent to a mass of approximately 50,000 kg. With this mass, QUE 90201 represents the largest stone meteorite identified on Antarctica, although other large objects may still remain to be discovered—in the form of unidentified chondrite showers—among the more than 30,000 Antarctic meteorites recovered. Based on the mass distribution of the QUE meteorites, we conclude that approximately 2000 small L and LL chondrites belong to the shower, which has a total recovered mass of approximately 65 kg, i.e., less than 0.2% of the incoming mass. The mass of the largest recovered fragment (~1.3 kg) is consistent with models of atmospheric fragmentation of small asteroids (Hills and Goda 1993; Bland and Artemieva 2006), while the low survival rate (<1% of the original mass) is consistent with a catastrophic breakup event (or multiple events) during atmospheric passage.

Acknowledgments—This work was supported, in part, by NASA grants NAG5-4992 (K. C. W. and K. N.), NAG5-9777 (T. J. M.), and a LLNL-CAMS grant. We thank the National Science Foundation for supporting the Antarctic Search for Meteorites (ANSMET) and the Meteorite Working Group for providing samples. We also are grateful to Bob Finkel for assistance with the AMS measurements at LLNL. AMS measurements at LLNL were performed under the auspices of the U.S. DOE by LLNL under contract W-7405-ENG-48. We thank Bernard Lavielle and Ingo Leya for valuable comments that improved this article, and Tim Jull for editorial handling.

Editorial Handling—Dr. A. J. Timothy Jull

REFERENCES

Ahn I., Choi C.-G., Park C. K., Lee J. I., and Wasson J. T. 2009. Bulk oxygen isotope compositions of equilibrated ordinary chondrite falls using CO_2 Laser-BrF_5 fluorination technique (abstract). *Meteoritics & Planetary Science* 44:A17.

Albrecht A., Schnabel C., Vogt S., Xue S., Herzog G. F., Begemann F., Weber H. W., Middleton R., Fink D., and Klein J. 2000. Light noble gases and cosmogenic radionuclides in Estherville, Budulan and other mesosiderites: Implications for exposure histories and production rates. *Meteoritics & Planetary Science* 35:975–986.

Aylmer D., Bonanno V., Herzog G. F., Weber H., Klein J., and Middleton R. 1988. ^{26}Al and ^{10}Be production rates in iron meteorites. *Earth and Planetary Science Letters* 72:247–262.

Begemann F., Weber H. W., Vilcsek E., and Hintenberger H. 1976. Rare gases and ^{36}Cl in stony-iron meteorites: Cosmogenic elemental production rates, exposure ages, diffusion losses and thermal histories. *Geochimica et Cosmochimica Acta* 40:353–368.

Benoit P. H., Sears D. W. G., Akridge J. M. C., Bland P. A., Berry F. J., and Pillinger C. T. 2000. The non-trivial problem of meteorite pairing. *Meteoritics & Planetary Science* 35:393–417.

Bland P. A. and Artemieva N. A. 2006. The rate of small impacts on Earth. *Meteoritics & Planetary Science* 41:607–631.

Bogard D. D., Nyquist L. E., Bansal B. M., Garrison D. H., Wiesmann H., Herzog G. F., Albrecht A. A., Vogt S., and Klein J. 1995. Neutron-capture ^{36}Cl, ^{41}Ca, ^{36}Ar and ^{150}Sm in large chondrites: Evidence for high fluences of thermalized neutrons. *Journal of Geophysical Research* 100:E9401–E9416.

Borovicka J. and Kalenda P. 2003. The Morávka meteorite fall: 4. Meteoroid dynamics and fragmentation in the atmosphere. *Meteoritics & Planetary Science* 38:1023–1043.

Brearley A. J. and Jones R. H. 1998. Chondritic meteorites. In *Planetary materials*, edited by Papike J. J. Washington, D.C.: Mineralogical Society of America. pp. 3-1–3-398.

Cassidy W., Harvey R., Schutt J., Delisle G., and Yanai K. 1992. The meteorite collection sites of Antarctica. *Meteoritics* 27:490–525.

Davis J. C., Proctor I. D., Southon J. R., Caffee M. W., Heikkinen D. W., Roberts M. L., Moore T. L., Turteltaub K. W., Nelson D. E., Loyd D. H., and Vogel J. S. 1990. LLNL/UC AMS facility and research program. *Nuclear Instruments and Methods in Physics Research B* 52:269–272.

Garrison D., Hamlin S., and Bogard D. 2000. Chlorine abundances in meteorites. *Meteoritics & Planetary Science* 35:419–429.

Gnos E., Lorenzetti S., Eugster O., Jull A. J. T., Hofmann B. A., Al-Kathiri A., and Eggimann M. 2009. The Jiddat al Harasis 073 strewn field, Sultanate of Oman. *Meteoritics & Planetary Science* 44:375–387.

Gomes C. B. and Keil K. 1980. *Brazilian stone meteorites*. Albuquerque, NM: University of New Mexico Press. 161 p.

Grady M. M. 2000. *Catalogue of meteorites*, 5th ed. Cambridge, UK: Cambridge University Press. 689 p.

Grossman J. N. 1994. The Meteoritical Bulletin, No. 76: The Antarctic meteorite collection. *Meteoritics* 29:A100–A143.

Grossman J. N. and Score R. 1996. The Meteoritical Bulletin, No. 79: Recently classified specimens in the U.S. Antarctic meteorite collection (1994–1996). *Meteoritics & Planetary Science* 31:A161–A174.

Halliday I., Blackwell A. T., and Griffin A. A. 1989. The flux of meteorites on the Earth's surface. *Meteoritics* 24:173–178.

Harvey R. P. 2003. The origin and significance of Antarctic meteorites. *Chemie der Erde* 63:93–147.

Hills J. G. and Goda M. P. 1993. The fragmentation of small asteroids in the atmosphere. *Astronomical Journal* 105:1114–1144.

Honda M., Nishiizumi K., Imamura M., Takaoka N., Nitoh O., Horie K., and Komura K. 1982. Cosmogenic nuclides in the Kirin chondrite. *Earth and Planetary Science Letters* 57:101–109.

Honda M., Caffee M. W., Miura Y. N., Nagai H., Nagao K., and Nishiizumi K. 2002. Cosmogenic nuclides in the Brenham pallasite. *Meteoritics & Planetary Science* 37:1711–1728.

Huber L., Gnos E., Hofmann B., Welten K. C., Nishiizumi K., Caffee M. W., Hillegonds D. J., and Leya I. 2008. The complex exposure history of the Jiddat al Harasis 073 L6 chondrite shower. *Meteoritics & Planetary Science* 43:1691–1708.

Huss G. R. 1991. Meteorite mass distributions and differences beteween Antarctic and non-Antarctic meteorites. *Geochimica et Cosmochimica Acta* 55:105–112.

Jarosewich E. 1990. Chemical analyses of meteorites: A compilation of stony and iron meteorites. *Meteoritics* 25:323–337.

Jenniskens P., Betlem H., Betlem J., Barifaijo E., Schlüter T., Hampton C., Laubenstein M., Kunz J., and Heusser G. 1994. The Mbale meteorite shower. *Meteoritics* 29:246–254.

Jull A. J. T. 2001. Terrestrial ages of meteorites. In *Accretion of extraterrestrial matter throughout Earth's history*, edited by Peucker-Ehrenbrink B. and Schmitz B. New York: Kluwer Academic/Plenum Publishers. pp. 241–266.

Keil K. and Fredriksson K. 1964. The iron, magnesium and calcium distribution in coexisting olivines and rhombic pyroxenes of chondrites. *Journal of Geophysical Research* 69:3487–3515.

Kenkmann T., Artemieva N. A., Wünnemann K., Poelchau M. H., Elbeshausen D., and Núñez del Prado H. 2009. The Carancas meteorite impact crater, Peru: Geologic surveying and modeling of crater formation and atmospheric passage. *Meteoritics & Planetary Science* 44:985–1000.

Klein J., Fink D., Middleton R., Nishiizumi K., and Arnold J. R. 1991a. Determination of half-life of ^{41}Ca from measurements of Antarctic meteorites. *Earth and Planetary Science Letters* 103:79–83.

Klein J., Fink D., Middleton R., Vogt S., and Herzog G. F. 1991b. ^{41}Ca in the Jilin H5 chondrite: A matter of size (abstract). *Meteoritics* 26:120.

Kong P. and Ebihara M. 1997. The origin and nebular history of the metal phase of ordinary chondrites. *Geochimica et Cosmochimica Acta* 61:2317–2329.

Kring D. A., Jull A. J. T., McHargue L. R., Bland P. A., Hill D. H., and Berry F. J. 2001. Gold Basin meteorite strewn field, Mojave Desert: Relict of a small Late Pleistocene impact event. *Meteoritics & Planetary Science* 36:1057–1066.

Langenauer M. and Krähenbühl U. 1993. Halogen contamination in Antarctic H5 and H6 chondrites and relation to sites of recovery. *Earth and Planetary Science Letters* 120:431–442.

Lavielle B., Marti K., Jeannot J.-P., Nishiizumi K., and Caffee M. W. 1999. The ^{36}Cl-^{36}Ar-^{40}K-^{41}K records and cosmic-ray production in iron meteorites. *Earth and Planetary Science Letters* 170:93–104.

Leya I. and Masarik J. 2009. Cosmogenic nuclides in stony meteorites revisited. *Meteoritics & Planetary Science* 44:1061–1086.

Leya I., Lange H.-J., Neumann S., Wieler R., and Michel R. 2000. The production of cosmogenic nuclides in stony meteoroids by galactic cosmic ray particles. *Meteoritics & Planetary Science* 35:259–286.

Leya I., Wieler R., Aggrey K., Herzog G. F., Schnabel C., Metzler K., Hildebrand A. R., Bouchard M., Jull A. J. T., Andrews H. R., Wang M.-S., Ferko T. E., Lipschutz M. E., Wacker J. F., Neumann S., and Michel R. 2001. Exposure history of the St-Robert (H5) fall. *Meteoritics & Planetary Science* 36:1479–1494.

Leya I., Welten K. C., Nishiizumi K., and Caffee M. W. 2009. Cosmogenic nuclides in the solar gas-rich H3–6 chondrite breccia Frontier Mountain 90174. *Meteoritics & Planetary Science* 44:77–85.

Masarik J. and Reedy R. C. 1994a. Effects of bulk composition on nuclide production processes in meteorites. *Geochimica et Cosmochimica Acta* 58:5307–5317.

Masarik J. and Reedy R. C. 1994b. Effects of meteoroid shape on cosmogenic nuclide production rates (abstract). 25th Lunar and Planetary Science Conference. pp. 843–844.

Masarik J., Nishiizumi K., and Reedy R. C. 2001. Production rates of cosmogenic helium-3, neon-21 and neon-22 in ordinary chondrites and the lunar surface. *Meteoritics & Planetary Science* 36:643–650.

McBride K. M. 2002. Statistical comparisons of Antarctic meteorites and falls (abstract #1323). 33rd Lunar and Planetary Science Conference. CD-ROM.

Metzler K., Ott U., Welten K., Caffee M. W., and Franke L. 2008. The L3–6 regolith breccia Northwest Africa 869: Petrology, noble gases and cosmogenic radionuclides (abstract #1120). 39th Lunar and Planetary Science Conference. CD-ROM.

Nagai H., Honda M., Imamura M., and Kobayashi K. 1993. Cosmogenic ^{10}Be and ^{26}Al in metal, carbon and silicate of meteorites. *Geochimica et Cosmochimica Acta* 57:3705–3723.

Nemtchinov I. V., Svetsov V. V., Kosarev I. B., Golub A. P., Popova O. P., Vhuvalov V. V., Spalding R. E., Jacobs C., and Tagliaferri E. 1997. Assessment of kinetic energy of meteoroids detected by satellite-based light sensors. *Icarus* 130:259–274.

Nishiizumi K. 2004. Preparation of ^{26}Al AMS standards. *Nuclear Instruments and Methods in Physics Research Section B* 223–224:388–392.

Nishiizumi K. and Caffee M. W. 1998. Measurements of cosmogenic calcium-41 and calcium-41/chlorine-36 terrestrial ages (abstract). *Meteoritics & Planetary Science* 33:A117.

Nishiizumi K., Klein J., Middleton R., and Arnold J. R. 1987. Long-lived cosmogenic nuclides in the Derrick Peak and Lazarev iron meteorites (abstract). 18th Lunar and Planetary Science Conference. pp. 724–725.

Nishiizumi K., Elmore D., and Kubik P. W. 1989a. Update on terrestrial ages of Antarctic meteorites. *Earth and Planetary Science Letters* 93:299–313.

Nishiizumi K., Kubik P. W., Elmore D., Reedy R. C., and Arnold J. R. 1989b. Cosmogenic ^{36}Cl production rates in meteorites and the lunar surface. Proceedings, 19th Lunar and Planetary Science Conference. pp. 305–312.

Nishiizumi K., Arnold J. R., Fink D., Klein J., and Middleton R. 1991. ^{41}Ca production profile in the Allende meteorite (abstract). *Meteoritics* 26:174.

Nishiizumi K., Caffee M. W., Jeannot J.-P., Lavielle B., and Honda M. 1997. A systematic study of the cosmic-ray exposure history of iron meteorites: Beryllium-10–chlorine-36/beryllium-10 terrestrial ages (abstract). *Meteoritics & Planetary Science* 32:A100.

Nishiizumi K., Caffee M. W., and DePaolo D. J. 2000. Preparation of ^{41}Ca AMS standards. *Nuclear Instruments and Methods in Physics Research B* 172:399–403.

Nishiizumi K., Imamura M., Caffee M. W., Southon J. R., Finkel R. C., and McAninch J. 2007. Absolute calibration of ^{10}Be AMS standards. *Nuclear Instruments and Methods in Physics Research B* 258:403–413.

Oddershedde L., Meibom A., and Bohr J. 1998. Scaling analysis of meteorite shower mass distributions. *Europhysics Letters* 43:598–604.

Rambaldi E. 1976. Trace element content of metals from L-group chondrites. *Earth and Planetary Science Letters* 31:224–238.

Rambaldi E. R. 1977. Trace element content of metals from H- and LL-group chondrites. *Earth and Planetary Science Letters* 36:347–358.

Reedy R. C. and Arnold J. R. 1972. Interaction of solar and galactic cosmic ray particles with the Moon. *Journal of Geophysical Research* 77:537–555.

Reedy R. C., Masarik J., Nishiizumi K., Arnold J. R., Finkel R. C., Caffee M. W., Southon J., Jull A. J. T., and Donahue D. J. 1993. Cosmogenic radionuclide profiles in Knyahinya: New measurements and models (abstract). 24th Lunar and Planetary Science Conference. pp. 1195–1196.

Rietmeijer F. J. M. and Nuth J. A. III. 2000. Collected extraterrestrial materials: Constraints on meteor and fireball compositions. *Earth, Moon, and Planets* 82–83:325–350.

Rubin A. E. 1990. Kamacite and olivine in ordinary chondrites: Inter-group and intra-group relationships. *Geochimica et Cosmochimica Acta* 54:1217–1232.

Scheirich P., Ďurech J., Pravec P., Kozubal M., Dantowitz R., Kaasalainen M., Betzler A. S., Beltrame P., Muler G., Birtwhistle P., and Kugel F. 2010. The shape and rotation of asteroid 2008 TC_3. *Meteoritics & Planetary Science* 45:1804–1811.

Sharma P., Kubik P. W., Fehn U., Gove G. E., Nishiizumi K., and Elmore D. 1990. Development of ^{36}Cl standards for AMS. *Nuclear Instruments and Methods in Physics Research B* 52:410–415.

Sharma P., Bourgeois M., Elmore D., Granger D., Lipschutz M. E., Max X., Miller T., Mueller K., Rickey F., Simms P., and Vogt S. 2000. PRIME lab AMS performance, upgrades and research applications. *Nuclear Instruments and Methods in Physics Research B* 172:112–123.

Spergel M. S., Reedy R. C., Lazareth O. W., Levy P. W., and Slatest L. A. 1986. Cosmogenic neutron-capture-produced nuclides in stony meteorites. *Journal of Geophysical Research* 91:D483–D494.

Vogt S., Aylmer D., Herzog G. F., Wieler R., Signer P., Pellas P., Fieni C., Tuniz C., Jull A. J. T., Fink D., Klein J., and Middleton R. 1993. On the Bur Gheluai H5 chondrite and other meteorites with complex exposure histories. *Meteoritics* 28:71–85.

Wasson J. T. and Kallemeyn G. W. 1988. Composition of chondrites. *Philosophical Transactions of the Royal Society of London* A325:535–544.

Welten K. C., Nishiizumi K., Caffee M. W., Schäfer J., and Wieler R. 1999. Terrestrial ages and exposure ages of Antarctic H chondrites from Frontier Mountain, North Victoria Land. *Antarctic Meteorite Research* 12:94–107.

Welten K. C., Nishiizumi K., Masarik J., Caffee M. W., Jull A. J. T., Klandrud S. E., and Wieler R. 2001a. Cosmic-ray exposure history of two Frontier Mountain H-chondrite showers from spallation and neutron-capture products. *Meteoritics & Planetary Science* 36:301–318.

Welten K. C., Bland P. A., Russell S. S., Grady M. M., Caffee M. W., Masarik J., Jull A. J. T., Weber H. W., and Schultz L. 2001b. Exposure age, terrestrial age and pre-atmospheric radius of the Chinguetti mesosiderite: Not part of a much larger mass. *Meteoritics & Planetary Science* 36:939–946.

Welten K. C., Nishiizumi K., Caffee M. W., Masarik J., Leya I., and Wieler R. 2002. Cosmogenic nuclides in metal and stone separates of an Antarctic L5/LL5-chondrite shower with a large pre-atmospheric size: QUE 90201 (abstract #1763). 33rd Lunar and Planetary Science Conference. CD-ROM.

Welten K. C., Caffee M. W., Leya I., Masarik J., Nishiizumi K., and Wieler R. 2003. Noble gases and cosmogenic radionuclides in the Gold Basin L4-chondrite shower: Thermal history, exposure history and pre-atmospheric size. *Meteoritics & Planetary Science* 38:157–173.

Welten K. C., Nishiizumi K., Caffee M. W., Hillegonds D. J., Johnson J. A., Jull A. J. T., Wieler R., and Folco L. 2006. Terrestrial age, pairing and concentration mechanism of Antarctic chondrites from Frontier Mountain, northern Victoria Land. *Meteoritics & Planetary Science* 41:1081–1094.

Welten K. and Nishiizumi K. 2007. Reclassifications. *Antarctic Meteorite Newsletter* 30:32.

Welten K. C., Caffee M. W., Hillegonds D. J., Masarik J., and Nishiizumi K. 2010a. Identifying large chondrites using cosmogenic radionuclides. *Nuclear Instruments and Methods in Physics Research B* 268:1185–1188.

Welten K. C., Caffee M. W., Leclerc M. D., Jull A. J. T., Metzler K., Franke L., and Ott U. 2010b. Evidence for recent near-catastrophic collision on large chondritic meteoroid, Northwest Africa 869 (abstract #2611). 41st Lunar and Planetary Science Conference. CD-ROM.

Zanda B., Bourot-Denise M., Perron C., and Hewins R. H. 1994. Origin and metamorphic redistribution of silicon, chromium and phosphorus in the metal of chondrites. *Science* 265:1846–1849.

APPENDIX

Terrestrial Age Methods

The ^{36}Cl/^{10}Be-^{10}Be Method

The ^{36}Cl/^{10}Be production rate ratio in the metal phase of meteorites varies from ~3.5 to ~6.0, and shows a good correlation with the ^{10}Be production rate (Nishiizumi et al. 1997). The correlation was determined for iron meteorites and the metal phase of stony and stony irons with CRE ages long enough to saturate both ^{36}Cl and ^{10}Be (Lavielle et al. 1999). After including recent results for the metal phase of Brenham (Honda et al. 2002), Chinguetti (Welten et al. 2001b), and Gold

Basin (Welten et al. 2003), we slightly modified the equation given earlier (Lavielle et al. 1999), as was discussed previously (Welten et al. 2006):

$$^{36}Cl/^{10}Be = 6.01 - 0.28 * [^{10}Be] - 0.009 * [^{10}Be]^2. \quad (A1)$$

The correlation of Equation A1 is based on iron meteorites and metallic phases of chondrites and stony irons with (on average) approximately 9 wt% Ni, whereas the metal fraction in many of the QUE L and LL chondrite samples in this study contains 20–30 wt% Ni. High Ni contents in the metal result in a lower ^{36}Cl production rate, as the elemental production rate of ^{36}Cl from Ni is approximately 25% lower than from Fe (Nishiizumi et al. 1989b). We thus corrected the measured ^{36}Cl concentrations in Table 2 to an average metal composition of 91% Fe and 9% Ni, based on measured Ni contents in the metal fraction of QUE samples (Table 1). Correction factors are 1.01–1.03 for L chondrites with <20 wt% Ni in the metal and 1.03–1.05 for LL (or L/LL) chondrites with 20–30 wt% Ni in the metal fraction. The $^{36}Cl/^{10}Be$ ratios in Table 2 include these corrections. Note that the $^{36}Cl/^{10}Be$-^{10}Be terrestrial age method is only reliable if the meteorite was exposed in space long enough (> 7 Myr), so that both ^{36}Cl and ^{10}Be were saturated at the time of fall. The degree of saturation at the time of fall can be estimated from the $^{26}Al/^{10}Be$ ratio in the metal fraction, which is constant at approximately 0.70 for irons and the metal of chondrites and stony irons (Aylmer et al. 1988; Lavielle et al. 1999; Albrecht et al. 2000)

We calculated the $^{26}Al/^{10}Be$ ratios at the time of fall from the measured $^{26}Al/^{10}Be$ ratios by correcting for radioactive decay of ^{26}Al and ^{10}Be during the terrestrial residence time. Most QUE chondrites show $^{26}Al/^{10}Be$ ratios of approximately 0.70, indicating minimum CRE age of 7 Myr. Two samples (QUE 93021 and 97429) show elevated $^{26}Al/^{10}Be$ ratios of approximately 0.9. QUE 93021 clearly has a short CRE age, as its $^{36}Cl/^{10}Be$ ratio is also higher than for falls, indicating undersaturation of ^{10}Be. For QUE 93021, we cannot calculate a reliable terrestrial age based on the $^{36}Cl/^{10}Be$-^{10}Be method. For QUE 97429, the high $^{26}Al/^{10}Be$ ratio does not seem to be due to an undersaturated ^{10}Be concentration, but to an elevated ^{26}Al concentration. A possible explanation is an unusually high concentration of phosphorus (~0.3 wt%) in the metal phase, as the production of ^{26}Al from P (relative to that from Fe and Ni) is more favorable at high shielding conditions. Zanda et al. (1994) have shown that the metal phase in chondrites of petrologic type 5 may contain P as tiny (<20 μm) phosphate grains. We thus assume that the $^{36}Cl/^{10}Be$-^{10}Be method yields a reliable terrestrial age for QUE 97429, as is confirmed by the results in Table 2. Uncertainties in the terrestrial ages include 1σ uncertainties in the measured ^{10}Be and ^{36}Cl concentrations, as well as an uncertainty of 3% in the $^{36}Cl/^{10}Be$ production rate ratio.

The $^{41}Ca/^{36}Cl$-^{36}Cl Method

The most reliable terrestrial age method for Antarctic meteorites with ages between ~40 and ~500 kyr is based on the correlation of the $^{41}Ca/^{36}Cl$ ratio versus the ^{36}Cl concentration (Nishiizumi and Caffee 1998). The $^{41}Ca/^{36}Cl$ method is much less dependent on the exposure history of a meteorite as long as the most recent CRE was > 1.5 Myr, which is valid for more than 99% of all ordinary chondrites. Although initial ^{36}Cl and ^{41}Ca measurements in the metal phase of a large number of meteorites showed an average $^{41}Ca/^{36}Cl$ ratio of 1.06 ± 0.13 (Nishiizumi and Caffee 1998), recent ^{41}Ca and ^{36}Cl measurements in the metal phase of the large Gold Basin L4 chondrite shower (Welten et al. 2003) suggest that the $^{41}Ca/^{36}Cl$ ratio increases to a value of 1.25 at higher shielding. For calculation of terrestrial ages based on the $^{41}Ca/^{36}Cl$ ratio, we adopted the following empirical correlation as shown in Welten et al. (2006). Note that the sign in the second term is positive instead of negative as was originally reported in Welten et al. (2006):

$$^{41}Ca/^{36}Cl = 1.25 + 0.003 * [^{36}Cl] - 0.0006 * [^{36}Cl]^2. \quad (A2)$$

Variations in the Ni concentration of the metal are not expected to affect the $^{41}Ca/^{36}Cl$ ratio significantly, as the reaction pathways for the production of ^{36}Cl and ^{41}Ca from Fe and Ni are very similar. Terrestrial ages of the QUE meteorites are given in Table 2. Uncertainties in the ages include 1σ uncertainties in the measured ^{36}Cl and ^{41}Ca concentrations, as well as an uncertainty of 5% in the $^{41}Ca/^{36}Cl$ production rate ratio.